Biomaterials Science

ROYAL SOCIETY OF CHEMISTRY

PAPER

View Article Online
View Journal | View Issue

Cite this: *Biomater. Sci.*, 2021, **9**, 5359

Electrical stimulation of neural-differentiating iPSCs on novel coaxial electroconductive nanofibers†

Fábio F. F. Garrudo, *[a,b,c,d] Diogo E. S. Nogueira, [b,c] Carlos A. V. Rodrigues, [b,c] Flávio A. Ferreira, [b,c] Patrizia Paradiso, [e] Rogério Colaço, [e] Ana C. Marques, [f] Joaquim M. S. Cabral, [b,c] Jorge Morgado, [d] Robert J. Linhardt *[a] and Frederico Castelo Ferreira *[b,c]

Neural tissue engineering strategies are paramount to create fully mature neurons, necessary for new therapeutic strategies for neurological diseases or the creation of reliable *in vitro* models. Scaffolds can provide physical support for these neurons and enable cues for enhancing neural cell differentiation, such as electrical current. Coaxial electrospinning fibers, designed to fulfill neural cell needs, bring together an electroconductive shell layer (PCL-PANI), able to mediate electrical stimulation of cells cultivated on fibers mesh surface, and a soft core layer (PGS), used to finetune fiber diameter (951 ± 465 nm) and mechanical properties (1.3 ± 0.2 MPa). Those dual functional coaxial fibers are electroconductive (0.063 ± 0.029 S cm^{-1}, stable over 21 days) and biodegradable (72% weigh loss in 12 hours upon human lipase accelerated assay). For the first time, the long-term effects of electrical stimulation on induced neural progenitor cells were studied using such fibers. The results show increase in neural maturation (upregulation of MAP2, NEF-H and SYP), up-regulation of glutamatergic marker genes (VGLUT1 – 15-fold) and voltage-sensitive channels (SCN1α – 12-fold, CACNA1C – 32-fold), and a down-regulation of GABAergic marker (GAD67 – 0.09-fold), as detected by qRT-PCR. Therefore, this study suggest a shift from an inhibitory to an excitatory neural cell profile. This work shows that the PGS/PCL-PANI coaxial fibers here developed have potential applications in neural tissue engineering.

Received 31st March 2021,
Accepted 22nd June 2021

DOI: 10.1039/d1bm00503k

rsc.li/biomaterials-science

1. Introduction

The brain is an electrically active organ, responsible for managing several key tasks paramount to the homeostasis of our body, including conscious ones (*e.g.* movement, balance, gesturing) and autonomic ones (*e.g.* sympathetic/parasympathetic response), along with more complex ones such as learning, thinking and judgement.[1,2] In neurological diseases, organ homeostasis is affected, and these key functions are compromised. Contrary to other organs, the regeneration potential of the brain is limited not only by the small stem cell pool available, but also by the complex neural cell architecture.[3] In particular, the brain tissue is composed by complex yet organized communication networks composed by neural cells from different lineages, including glutamatergic, GABAergic and dopaminergic ones. This functionally dynamic network is established throughout the whole life of the individual and its composition varies according to the brain region. For example, the cerebral cortex is dominated by glutamatergic and GABAergic neurons, whereas the substancia nigra is dominated by GABAergic and dopaminergic neurons.[4–6]

Tissue engineering/Regenerative medicine strategies make use of multidisciplinary approaches (*e.g.* cell biology, biomaterials, nanotechnology) to create replacements for damaged tissues. Recreating the normal neural architecture *in vitro* can

[a]*Department of Chemistry and Chemical Biology, Department of Chemistry & Chemical Biology, Rensselaer Polytechnic Institute, Biotechnology Center 4005, Troy, NY, 12180, USA. E-mail: fabio.garrudo@campus.ul.pt, linhar@rpi.edu*
[b]*Department of Bioengineering and iBB – Institute for Bioengineering and Biosciences, Instituto Superior Técnico, Universidade de Lisboa, Av. Rovisco Pais, 1049-001 Lisboa, Portugal. E-mail: frederico.ferreira@tecnico.ulisboa.pt*
[c]*Associate Laboratory i4HB—Institute for Health and Bioeconomy, Instituto Superior Técnico, Universidade de Lisboa, Av. Rovisco Pais, 1049-001 Lisboa, Portugal*
[d]*Department of Bioengineering and Instituto de Telecomunicações, Universidade de Lisboa, Av. Rovisco Pais, P-1049-001 Lisboa, Portugal*
[e]*IDMEC - Instituto de Engenharia Mecânica, Instituto Superior Técnico, Universidade de Lisboa, Av. Rovisco Pais, P-1049-001 Lisboa, Portugal*
[f]*CERENA, DEQ, Instituto Superior Técnico, Universidade de Lisboa, Avenida Rovisco Pais, P-1049-001 Lisboa, Portugal*

†Electronic supplementary information (ESI) available. See DOI: 10.1039/d1bm00503k

ultimately be used to design artificial tissues that can potentially be transplanted to a diseased brain, such as one afflicted by neurodegenerative diseases, or used as disease models to test novel therapeutic approaches.[7–9] This can ultimately reduce the risk of rejection and boost the recovery of patients. Different neural tissue engineering strategies can be used to achieve this goal, including the use of stem cells, physicochemical cues and even scaffolds.[10–12]

Fully matured and differentiated neurons can be obtained from induced pluripotent stem cells (iPSCs).[13] iPSCs were first derived from somatic cells through reprogramming, which allows them to overcome some of the ethical issues associated with embryonic stem cells.[14] iPSCs are also able to self-renew and can generate cells from the three germ layers found in the developing embryo.[15] Several protocols describe the neural induction of iPSCs into induced neural progenitor cells (iNPCs), which can then be differentiated into neural cells.[16] Due to their high quality, these cells are trustworthy *in vitro* disease models[17,18] and can potentially be directly transplanted into patients for the treatment of neurological diseases.[19,20] However, the protocols used to generate neurons are generally laborious and time-consuming (up to 120 days) and the homogeneity of the obtained cell population is dependent on the quality and timing of the chemical cues used.[21–23]

Electrical stimulation is a powerful cue that can be used to enhance neural cell differentiation. This cue affects the normal membrane potential of the cells due to the presence of voltage-sensitive proteins responsible for ion movement. Membrane potential and genetic pathways are interconnected, and together affect metabolism, cell cycle stage and differentiation progression. In fact, electrical stimulation was previously shown to enhance neural stem cell (NSC) proliferation,[24,25] neural cell morphology[26] and secretome.[27] Regarding neural differentiation, electrical stimulation can enhance neural cell elongation,[28] increase the number of neurons[29] and also the expression of mature neural markers.[30,31] Nevertheless, little is known on how electrical stimulation can affect differentiation of neural cells in the long-term, and more specifically on the iPSC differentiation into lineage-specific neurons.

Electroconductive polymers are able to conduct electrical stimuli. When used in scaffolds that support neural cell culture, they allow direct and effective electrical stimulation of cultured cells. Electroconductive polymers possess several advantages in the production of neural-friendly platforms. Contrary to metals such as platinum or gold, they possess reduced and tailored stiffness, improved tissue integration,[32] ease of functionalization through blending[33] or chemical immobilization of bioactive moieties[34] and the ability to be processed/tailored into different topographic/3D structure that mimics the target tissue architecture[35,36] and promotes cell integration.[37] One example of such is Poly(aniline) (PANI) doped with camphorsulfonic acid (CSA), a cheap, non-biodegradable and yet highly electroconductive material whose electroconductivity can be enhanced through the use of specific solvent mixtures.[31]

The ability of cells to remodel the substrate in which they are cultured is beneficial for the maintenance of NSCs stemness[38] and enhancing their differentiation into neurons.[39] Electroconductive polymers are not biodegradable. As such, an ideal platform for studying the neural differentiation of iPSCs should also be composed by biodegradable components, such as Poly(caprolactone) (PCL) and/or poly(glycerol sebacate) (PGS).[40,41] PCL is a synthetic aliphatic polyester, FDA approved, biodegradable and with good thermoplastic properties that make it easily processed. PCL can also be blended with PANI in an electroconductive blend ($1.9 \pm 0.4 \times 10^{-1}$ S cm^{-1}) suitable for the electrical stimulation of NSCs.[31] PGS is another synthetic aliphatic polyester, easily synthesizable with FDA approved materials (glycerol and sebacic acid), biodegradable and suitable for tissue engineering applications.[40]

There are different techniques that can be employed in the production of neural-friendly scaffolds. Electrospinning is a versatile technique that allows the production of nanofibers from polymer solutions. The obtained electrospun fibers can mimic the topography of the natural extracellular matrix (ECM)[3] due to their small diameter, high porosity and high surface areas, which can improve cell differentiation[42–44] and promote the production of a more mature and dynamic ECM by cultured cells.[45] Previous reports show that electrospun scaffolds can support iPSC growth,[46] promote *in situ* iPSC-derived cardiomyocyte differentiation[47] and improve the success of transplanting *in vitro* generated neural networks into the mouse brain striatum.[37] Moreover, monoaxial fibers can support the initial stages of neural differentiation of iPSCs.[48]

Polymers that yield solutions with very low viscosities (*e.g.* PGS) cannot be directly electrospun.[49] In this case the most viable strategy is the encapsulation of the desired polymer (PGS) in a coaxial structure while using an electrospinnable polymer for the shell layer (*e.g.* PCL).[50,51] This strategy is named coaxial electrospinning and allows to obtain double layer fibers that can ben chemically/functionally different. Thus, using this strategy it is possible to create coaxial fibers with an outer electroconductive layer, that can conduct electrical stimulation directly to the cultured cells, and an inner layer for support. Such supporting layer confers other advantages to the obtained fibers, including higher diameters, possibility of tailoring the mechanical properties of the fibers and enable the encapsulation of unstable/sensitive active molecules in the fiber core for further controlled release.[52] While the number of available reports on coaxial electrospun fibers is vast,[53,54] its applicability in tissue engineering, specifically as electroconductive and biodegradable scaffolds for neural tissue,[55–57] has not been well developed.

Our group has developed diverse PGS/PCL coaxial fibers for tissue engineering applications.[58,59] Some of their features were hypothesized to favor neural cell differentiation, including high diameters (larger than 750 nm), low Young's module (4–16 MPa) and biodegradability. Moreover, their coaxial structure could potentially be used in the future for developing multifunctional systems, including platforms for controlled

drug release platforms. Therefore, we proposed to produce an electroconductive version of these fibers that could be suitable for neural cell differentiation. Prior this work, we successfully optimized the preparation of the composites for the shell layer, by determining (1) the best PCL to PANI ratio for the best electroconductivity : biocompatibility relationship,[60] and (2) the best solvent system for PCL-PANI composite to further enhance electroconductivity and allow fiber production to be more reliable.[31]

The first goal of this work is to therefore develop coaxial electrospun fibers that are both biodegradable and electroconductive that can be used to electrically stimulate neural differentiating iPSCs *in vitro*. Such fibers are composed of a shell layer of PCL-PANI, for electrical conduction, and a core layer of PGS, which allows to finetune fiber diameter and mechanical properties. We then performed cell studies on the coaxial fibers using iPSC-derived neural cells to investigate the effects of electrical stimulation on neural differentiation and the predominant neural lineage of the cells obtained. The approach described is particularly important for the treatment of currently incurable neurological diseases, such as neurodegenerative ones.

2. Experimental section

2.1. Materials

PANI (emeraldine base), of molecular weight (MW) 100 000 Da, CSA (98% purity), 2,2,2-trifluoroethanol (CF_3CH_2OH, TFE), 1,1,1,3,3,3-hexafluoropropanol ($CF_3CH(OH)CF_3$, HFP), PCL of MW 80 000 Da, glycerol (>99.5%), sebacic acid (99%), titanium (II) oxide powder, Lipase (EC 3.1.1.3) from Aspergillus oryzae (~50 U mg^{-1}), SYLGARD® 184 Silicone elastomer (poly(dimethylsiloxane)), poly(L-ornithine hydrobromide) MW 30 000–70 000 Da (poly(ornithine)), glucose, human recombinant insulin, ethylene diamine tetra–acetic acid (EDTA) solution, SB-431542, dimethylsulfoxide (DMSO), 2-(4-amidinophenyl)-6-indolecarbamidine dihydrochloride (DAPI), paraformaldehyde (PFA) (crystalline) and the primary antibodies Anti-β3-Tubbulin (Anti-TUJ1) (mouse) (T8578), Anti-Microtubule Associated Protein (Anti-MAP2) (mouse) (AMAB91375) and Anti-vesicular γ-aminobutyric acid (GABA) transporter (Anti-VGAT) (rabbit) (HPA058859) were purchased from Merck (Darmstadt, Germany). Dulbecco's phosphate buffered saline (PBS), Dulbecco's Modified Eagle's Medium (DMEM-F12+Glutamax (1X)), Antibiotic–Antimycotic (Anti–Anti) mixture (penicillin 10 000 units per mL, streptomycin 10 000 μg mL^{-1}, Amphotericin B 25 μg mL^{-1}), Penicillin–Streptomycin (Pen–Strep) mixture (penicillin 10 000 units per mL, streptomycin 10 000 μg mL^{-1}), N2-supplement (100X), B27-supplement (50X), neurobasal medium, Triton-X-100 (Surfact-Amps®, 10% in water), primary antibodies Anti-*Zonula Occludens* (Anti-ZO1) (rabbit) and Anti-Neural Nuclear protein (Anti-NEUN) (rabbit) (702022), secondary antibodies Alexa 488 anti-mouse IgG, Alexa 488 anti-mouse IgM and Alexa 546 anti-rabbit IgG, High-Capacity cDNA Reverse Transcription Kit and MicroAmp Fast Optical 96-well reaction plates, were obtained from Thermo Fisher Scientific (Waltham, MA, USA). Ultra-low attachment 24-well plates (flat bottom) and Matrigel were obtained from Corning Inc. (Corning, NY, USA). mTeSR1 and ROCK inhibitor Y-27632 were purchased from STEMCELL Technologies (Vancouver, Canada). Human recombinant fibroblast growth factor 2 (FGF-2) was purchased from PeproTech EC, Ltd (London, UK). The primary antibody Anti-Podocalyxin (Anti-TRA-1-60) (rabbit) was acquired from Miltenyi Biotec (Bergisch Gladbach, Germany). The primary antibody Anti-Stage Specific Embryo Antigen 4 (Anti-SSEA-4) (rabbit) and LDN193189 were acquired from Stemgent (Cambridge, MA, USA). The primary antibody Anti-(Sex determining region Y)-box 2 (Anti-SOX2) (rabbit) (orb607714) was purchased from Byorbyt (Cambridge, UK). The primary antibody Anti-Nestin (Anti-NES) (mouse) (MAB1259) was purchased from R&D systems (Minneapolis, MN, USA). The primary antibodies Anti-Neurofilament M/H (Anti-NEF) (mouse) (801901), Anti-Paired box protein 6 (Anti-Pax6) (rabbit) (901301), Anti-Synaptophysin (Anti-SYP) (mouse IgM) (837103) and Anti-vesicular glutamate transporter 1 (Anti-VGLUT1) (mouse IgG1) (821301) were purchased from BioLegend (San Diego, CA, USA). RNA extraction kit RNeasy Mini was purchased from Qiagen (Hilden, Germany). qPCR master mix NZYSpeedy green ROX plus was obtained from Nzytech (Lumiar, Lisboa, Portugal). TcLab (F002.1A.13 cell line, originally reprogrammed from human healthy fibroblasts (46, female donor) through retroviral transduction of human genes OCT4, SOX2, C-MYC and KLF4) cells were acquired from Tecnologias Celulares para Aplicação Médica (Évora, Portugal).

2.2 PGS and solution preparation

PGS was prepared following the protocol of Hou and colleagues.[59] Briefly, 1 : 1 molar ratio of sebacic acid and glycerol were mixed at 130 °C under a nitrogen atmosphere for 3 h and then reacted at 120 °C under high vacuum (approximately 50 mTorr) for 25 h. PGS was then left to cool down in a desiccator to reduce moisture absorption and used without further processing. PCL solution was prepared by dissolving PCL (1.3 g) in TFE : HFP 5 : 5 (10 mL) mixture and left to agitate for 24 h. For PCL-PANI appropriate amounts of PANI (68 mg) and CSA (87 mg) were dispersed into a TFE : HFP 5 : 5 (10 mL) mixture and left to agitate for 24 h. PCL (1.3 g) was then added and left to agitate for more 24–48 h. PGS solution (80%) was prepared by dissolving PGS (8.0 g) in HFP (10 mL). The summary for the composition of each solution can be found in Table S1.†

2.3. Electrospinning

The prepared PCL and PCL-PANI solutions were electrospun using a spinneret system (MECC, Ogori, Fukuoka, Japan) (Fig. 1A) and a 23G needle (0.635 mm of internal diameter) under the following conditions: voltage of 15 kV, flow rate at 1 mL h^{-1}, distance from needle to collector of 15 cm, temperature of 21 °C, relative humidity of 50–60%. For PGS/PCL-PANI fibers a coaxial spinneret (MECC, Ogori, Fukuoka, Japan)

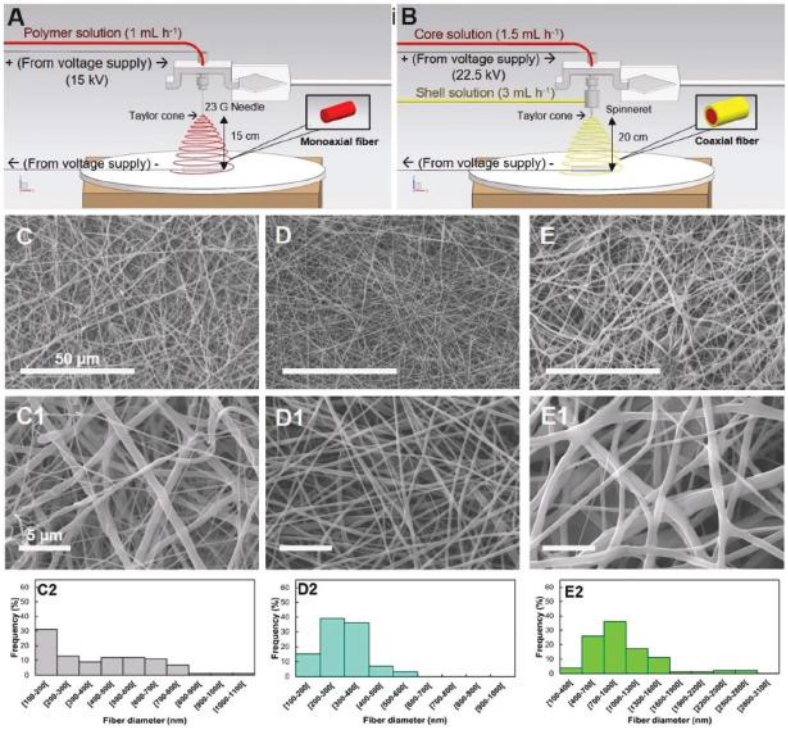

Fig. 1 Schematics of the electrospinning setups used for the production of (A) monoaxial and (B) coaxial fibers. PCL (C1 and C2), PCL-PANI (D1 and D2) and PGS/PCL-PANI 13% electrospun fibers (E1 and E2), and respective histograms (C3, D3 and E3) (n = 100).

(2.5 mm of internal diameter) was inserted in the electrospinning setup using a 23G needle as the internal (Fig. 1B). Electrospinning was conducted in the following conditions: shell solution (PCL-PANI) flow rate at 3 mL h^{-1}, core solution (PGS 80%) flow rate at 1.5 mL h^{-1}, voltage of 22.5 kV, distance to the collector of 20 cm, temperature of 21 °C, relative humidity of 40–50%. An air-blower was used to force fiber deposition on the collector.

2.4. Fiber morphology

2.4.1 Scanning electron microscopy (SEM). The morphology of the produced electrospun fiber mats was evaluated using a FEG-SEM JEOL JSM7001F (Jeol, Akishima, Tokyo, Japan) at 5 kV, after coating with a thin layer of gold/palladium. Fiber mat cross-sections and morphology after the stability assays were evaluated using a Hitachi S-2400 SEM (Hitachi, Chiyoda, Tokyo, Japan) at 20 kV, after coating with a thin layer of gold/palladium. The average diameter of the electrospun fiber samples was determined from SEM pictures of 100 individual fibers (20 fibers per each of 5 images) using NIH ImageJ software (National Institute of Health, MD, USA). The diameters obtained were averaged and used to plot the respective histograms.

2.4.2. Transmission electron microscopy. To improve the contrast of the coaxial fiber core, titanium dioxide (TiO_2) (50 mg mL^{-1}) was added to the original PGS 80% solution before electrospinning. PGS/PCL-PANI samples containing TiO_2 were then visualized by TEM (HITACHI H-8100, 200 kV high voltage and LaB6 Filament).

2.5. Fiber physico-chemical properties

2.5.1. Differential scanning calorimetry (DSC). DSC analysis was performed for PCL, PCL-PANI and PGS/PCL-PANI fibers using a Netzsch DSC-200-F3 Maia® (Netzsch Holding, Selb, Germany). DSC was performed at 5 °C min^{-1} from −30 °C to 100 °C for 2 cycles and finally until 420 °C for the final cycle. Data obtained was analyzed with the Software NETZSCH Proteus®.

2.5.2. Attenuated total reflectance-Fourier transform infrared spectroscopy (ATR-FTIR). The analysis of the fibers mats was performed using a Spectrum Two FT-IR Spectrometer (PerkinElmer, Waltham, MA, USA), equipped with a Pike Technologies MIRacle® ATR accessory. Transmittance spectra were obtained over the region from 400 to 4000 cm^{-1} (resolution of 4 cm^{-1}, 8 scans) at room temperature and an automatic baseline correction treatment was applied using the acquisition software.

2.5.3. 4-Point probe electroconductivity measurement. Four 50 nm thick gold stripes were deposited using a thermal evaporation system Edwards Coating System E 306A (Edwards, Irvine, CA, USA) to improve the electrical contact between the samples (PCL-PANI and PGS/PCL-PANI) and the measurement

equipment. The electroconductivity of three different films was measured by the four-point probe method, using a current source Keithley DC power source (Keithley Instruments, Cleveland, OH, USA) and a multimeter Agilent 34401A Multimeter (Agilent Technologies, Santa Clara, CA, USA). Finally, the thickness of the fiber mats was measured using a caliper.

2.5.4. Contact angle. Determination of the contact angle of the fiber mats was performed by a Krüss DSA25B goniometer (Krüss GmbH, Hamburg, Germany), using the sessile drop technique (glycerol). The spreading of the droplet on different fiber mats was assessed by measuring the contact angle of the droplet with the surface (n = 6). Drop Shape Analysis 4 Software was instructed to take measurements of the left and right angles every 5 s for 2 min.

2.5.5. Mechanical properties. A uniaxial tensile test was performed on the electrospun mats using a texture analyzer TA.XT ExpressC (Stable Micro Systems, Godalming, UK) equipped with 50 N tensile grips. Specimens were cut into rectangular strips (40 mm × 10 mm, n = 5) and the crosshead speed was set constant at 30 mm min^{-1} during the uniaxial test. Young's modulus was calculated from the 0–15% strain linear region in the stress–strain curve and the ultimate tensile strength and maximum extension were measured from the highest peak of the stress–strain curve.

2.6. Fiber stability

2.6.1. Lipase assay. Stability was evaluated in a sterile PBS solution containing lipase (EC 3.1.1.3) expressed in *Aspergillus oryzae* (0.5 U mL^{-1}), at 37 °C and 5% CO_2 for 1 h, 4 h, 8 h, 12 h, 24 h, 48 h and 168 h (7 days). Samples were collected, weighed, and treated similarly to those of the PBS stability assay. Mass Remaining (MR) (eqn (1)), water content (WC) (eqn (2)), pH of the obtained solutions (827 pH lab, Metrohm, Herisau, Switzerland), fiber diameter, FTIR profile and electroconductivity (4 h, 24 h and 168 h) were used as outcomes to evaluate degradation.

2.6.2. PBS assay. The stability of the obtained fiber mats was evaluated in PBS. Briefly, specimens were cut into rectangular strips (40 mm × 10 mm, n = 3), weighed and incubated with sterile PBS (37 °C, 5% CO_2) for 4, 7, 14, 21 and 28 days. The collected samples were washed with distilled water three times and then excess water was removed before initial weighting. Next, samples were dried at 45 °C for at least 24 h and then until constant weight, *i.e.*, until three successive measurements, approximately 12 h apart, varied ± 1%. Mass Remaining (MR) (eqn (1)) and water content (WC) (eqn (2)) were calculated for the samples following the equations:

$$\mathrm{MR} = [(\text{final weight})/(\text{initial weight})] \times 100 \quad (1)$$

$$\mathrm{WC} = [(\text{wet weight} - \text{dry weight})/(\text{wet weight})] \times 100 \quad (2)$$

Finally, the pH of the obtained PBS solutions, fiber diameter, FTIR profile and the electroconductivity of the samples were also evaluated.

2.7. Cell culture assays

2.7.1. Induced pluripotent stem cell (iPSC) culture. Thawed iPSCs (passage 41) were cultured on 6-well plates coated with Matrigel (1 : 100) in mTeSR1 culture medium, with daily medium replacement. Passage was performed when cells reached 80–90% confluency by incubation with EDTA (0.5 mmol L^{-1}) for 5 minutes at RT, after washing twice with EDTA solution. Cells were collected by pipetting with culture medium and divided in a split ratio of 1 : 3 to new Matrigel coated 6-well plates (passage 42). Passage was repeated a second time and cells were divided in a split ratio of 1 : 2 (passage 43) and left to grow until 90–100% confluency was reached.

2.7.2. IPSC commitment into induced neural progenitor cells (iNPCs). iPSC neural induction protocol was adapted from Shi and colleagues[16] and was performed through the dual-SMAD inhibition protocol.[23,61] Differentiation of iPSCs into iNPCs was initiated after cell confluency was reached. Medium was exchanged to N2B27 and then changed daily for 11 consecutive days. N2B27 medium is composed by a 1 : 1 mixture of N2 and B27 media. N2 medium is composed of DMEM/F12 with N2 supplement (1 : 100) additional glucose (1.6 g mL^{-1}), insulin (20 μg mL^{-1}) and pen-strep (1 : 100), while B27 medium is composed of Neurobasal medium, B27 supplement (2 : 100), Glutamax (1 : 100) and pen-strep (1 : 200). During the first 12 days of differentiation, N2B27 medium was supplemented with SB-431542 (10 μM) and LDN-193189 (100 nM). At day 12, the obtained iNPCs were passaged (EDTA solution) to new 6-well plates pre-coated with poly(ornithine) (20 μg mL^{-1}) and laminin (10 μg mL^{-1}). Cells were replated in a split ratio of 1 : 1 and N2B27 medium was changed daily. After day 14, after confirming the presence of neural rosettes, N2B27 medium was supplemented with FGF-2 (10 ng mL^{-1}) to promote cell proliferation until day 17.

2.7.3. iNPC differentiation on electrospun fibers. The electrospun fiber mats, fixed to glass coverslips with medical glue, were UV sterilized for 1.5 h per scaffold side and then glued to a non-adherent plate overnight. To ensure complete solvent removal, the scaffolds were incubated with 1% anti–anti solution in DMEM-F12 (37 °C, 5% CO_2) for 1 h thrice or until the color was consistently red (pH ≈7.4). Next, scaffolds were washed and incubated with a 1% anti–anti solution in PBS overnight (37 °C, 5% CO_2). Coating with poly(ornithine) (20 μg mL^{-1}) and laminin (1 μg mL^{-1}) was performed before seeding of the cells. iNPCs at day 17 were detached by incubation with EDTA, resuspended in N2B27 medium (2 mL per well), passaged to the fibers (60 μL per sample) already containing N2B27 medium (500 μL) and left to differentiate on N2B27 medium for more 30 days, with no additional factors added. Cell medium was changed at day 1 after seeding and then only half of the cell media was changed every 2 days until the end of the assay.

2.8. Electrical stimulation assay

The electrical stimulation setups used were similar to the ones used in our previous work.[31] Briefly, parallel gold contacts

(1 cm apart) were deposited, hollow 3D-printed ABS cylinders were glued in the space between using PDMS and platinum wires were glued to the gold contacts using silver paste. Setups were then sterilized through UV radiation and incubation with anti–anti 1% (in PBS) solution at 37 °C for 3 h, and then coated with poly(ornithine) and laminin before iNPC seeding (day 17). Electrical stimulation was performed from day 18 to day 47 on the following regime: pulsatile direct-current (pDC), 1 V cm^{-1} (1 V applied between 2 electrodes 1 cm apart), 100 Hz. Cell samples were collected 15 and 30 days after seeding for further analysis.

2.9. Cell analysis

2.9.1. Flow cytometry. Flow cytometry analysis was performed on days 0, 12 and 17 of differentiation. Briefly, cells were dissociated using EDTA (5 min) and fixed with PFA 2% for 20 min. The cells were then stained using previously described protocols for intracellular[62] (OCT4 and SOX2) and surface[63] (TRA-1-60 and SSEA-4) markers. Goat anti-mouse IgG 488 was used both as a secondary antibody and as a negative control for intracellular markers. The gate was selected to contain 1% of false positives (*i.e.*, 1% of the negative control samples).

2.9.2. Immunofluorescence. iPSCs (day 0), iNPCs (days 12 and 17) and neurons on electrospun scaffolds (days 30 and 47) were first washed with PBS and fixed in PFA 4% for 10 min. *Intracellular markers*: Cells were washed with PBS twice and permeabilized with blocking solution (goat serum 10% and Triton-x-100 0.2% in PBS) for 15 min at RT. After another washing with PBS, each cell sample was incubated with their respective antibodies. Anti-MAP2 (1 : 200), Anti-NEF (1 : 500), Anti-NES (1 : 250), Anti-NEUN (1 : 200) Anti-OCT4 (1 : 150), Anti-PAX6 (1 : 250), Anti-SOX2 (1 : 100), Anti-SYP (1 : 500), Anti-TUJ1 (1 : 400), Anti-VGAT (1 : 100), Anti-VGLUT1 (1 : 200), Anti-ZO1 (1 : 100), and were diluted in staining solution (goat serum 5% and Triton-x-100 0.1% in PBS) and the cells were incubated overnight at 4 °C. This was followed by incubation with the secondary antibodies Alexa 488 anti-mouse and/or Alexa 546 anti-rabbit (1 : 250) diluted in staining solution for 1 h at RT. *Surface markers*: samples were washed with PBS and non-permeabilizing blocking solution (goat serum 10% in PBS) for 15 min at RT. After another washing with PBS, cells were incubated with the antibodies. Anti-TRA-1-60 (1 : 135) and Anti-SSEA4 (1 : 135) were diluted in non-permeabilizing staining solution (goat serum 5% PBS) and cells were incubated with them overnight at 4 °C. This was followed by incubation of the secondary antibodies Alexa 546 anti-rabbit (1 : 250) diluted in staining solution for 1 h at RT. *All Markers*: all samples were counter-stained with DAPI (1 mg mL^{-1} diluted in staining solution) for 5 min at RT. Cells were then washed, kept in PBS, and imaged using a Leica DMI 3000B fluorescence microscope (Leica camera, Wetzlar, Germany).

VGLUT1 and VGAT fluorescence intensity was quantified using ImageJ software. Briefly, fluorescent images of both markers were collected and refined using the same settings for fluorescence intensity and contrast before being converted to 8 bits images. Fluorescence quantification from the whole image area and background were selected for each of the markers and DAPI from 5 independent images. The calculated corrected total fluorescence (CCTF) was calculated from these values using the following equation:

$$\mathrm{CCTF} = \text{Integrated density} - (\text{Area selected} \times \text{mean fluorescence of background reading}) \quad (3)$$

The obtained CCTF values for VGLUT1 and VGAT were then normalized to the corresponding CCTF for DAPI to obtain the corresponding *Fluorescence normalized to DAPI* (n = 5) and plotted.

2.9.3. Cell sample preparation for SEM. Fixed cells were dehydrated by incubation (30 min per step) with increasingly concentrated ethanol solutions (10%, 30%, 50%, 70%, 90% and 96%). Cell drying was performed by incubating (30 min per step) the obtained cells with increasing amounts of HMDS to 96% ethanol (1 : 2, 1 : 1, 2 : 1). Finally, cells were left in pure HMDS and left to dry at RT in a fume hood. Cells were then coated with gold/palladium and imaged using SEM.

2.9.4. Quantitative real-time polymerase chain reaction (qPCR). qPCR was performed using SYBR® Green chemistry. Primer construction was performed for the human genes Octamer-binding transcription factor 4 (OCT4) (iPSCs), SOX2 (iPSCs and NPCs), NES (NPCs), PAX6 (Radial Glia), T-box brain protein 2 (TBR2) (intermediate neural progenitor cells), T-box brain protein 1 (TBR1) (post-mitotic neurons), doublecortin (DCX) (newborn/migratory neurons), β-3 tubulin (TUBB3) (neurons – early marker), neurofilament light polypeptide (NEF-L) (neurons – mature marker), neurofilament medium polypeptide (NEF-M) (neurons – mature marker), neurofilament heavy polypeptide (NEF-H) (neurons – mature marker), MAP2 (neurons – mature marker), microtubule-associated protein tau (TAU) (neurons – mature marker), NEUN (neurons – mature marker), neural cell adhesion molecule (NCAM) (neurons – mature marker), SYP (neurons – mature marker) glutamate decarboxylase 67 (GAD67) and vesicular GABA transporter (VGAT) (GABAergic neurons), tyrosine hydroxylase (TH) and dopamine receptor D2 (DRD2) (dopaminergic neurons), vesicular glutamate transporter 1 (VGLUT1) and VGLUT2 (glutamatergic neurons), voltage-dependent L-type calcium channel subunit alpha-1C (CACNA1C) (calcium channel component) and sodium voltage-gated channel alpha subunit 1 (SCN1α) (sodium channel component). Briefly, the respective human (GRCh38.p13) cDNA transcript sequences for each gene tested were obtained from e!Ensembl.org. Next, primer design was performed using Primer3 (v. 0.4.0) for the best sequences, SnapGene® Viewer (5.0.7) for transcript size and Tm evaluation and e!Ensembl.org for cDNA BLASTN. The sequences for PAX6 were used from Paşca and colleagues[17] while the sequences of TBR2 and GAPDH (internal control) were used from Silva and colleagues.[64] The primer sequences used can be found in the ESI Table S2.† Gene expression at days 0, 12 and 17 of iPSC differentiation into iNPCs, and days

15 and 30 of iNPCs differentiation into neurons on the fibers/setups was determined using the comparative Ct method and by normalizing the expression of each target gene to the endogenous reference transcript GAPDH.

2.10. Data analysis and visualization

2.10.1. Statistical analysis. All data are presented as mean values ± standard deviations (std) or standard error of the mean (sem) for qPCR. Statistical analysis was performed using Microsoft Excel. Significant differences between groups were measured using ANOVA test, followed by *post-hoc* analysis and Bonferroni correction. $p < 0.05$ was considered statistically significant.

2.10.2. Data plotting. Graphics were plotted using Microsoft Excel®. Images were constructed using Microsoft PowerPoint®.

3. Results

3.1. Fiber morphology and physico-chemical characterization

We were able to obtain continuous and smooth fibers for all samples produced. The SEM images of the fiber mats and their diameter distribution can be seen in Fig. 1. Fiber diameter changes dramatically among the samples prepared. Initially, PCL fibers produced with the solvent system TFE : HFP 5 : 5 have a lower diameter (397 ± 235 nm) and are more heterogeneous than the produced in our previous study (561 ± 187 nm) where TFE alone was used.[60] Interestingly, the addition of PANI : CSA to the PCL fibers leads to a slight decrease in PCL-PANI fiber diameter (296 ± 93 nm), as observed in our previous work.[60] For the coaxial fibers, their diameter increases (951 ± 465 nm) due to the presence of encapsulated PGS.

The next step was to evaluate the presence of a coaxial structure in the fibers using TEM and evaluation of the fibers cross-sections by SEM. For TEM imaging, fiber contrast was first improved using a dispersion of TiO_2 nanoparticles in the core layer, which could be later observed as depicted in Fig. 2A and 2A1-2. For SEM, samples were cut in liquid nitrogen to freeze PGS and allow the fibers to maintain an intact coaxial structure, which was later observed as it can be seen in Fig. 2B1-4. An interesting feature observed is the presence of a coaxial structure in all the fibers visualized independently of the corresponding diameter. Overall, both SEM and TEM evidence the coaxial structure of the PGS/PCL-PANI fibers, irrespective of their diameter.

The FTIR spectra of the fibers produced and the original PGS raw material are shown in Fig. 3A. The spectrum for the PCL fibers shows peaks corresponding to the characteristic fingerprint region (900–1500 cm^{-1}), carbonyl groups (1725 cm^{-1}) and C–H symmetric/asymmetric stretching of CH_2 groups (2863 cm^{-1} and 2938 cm^{-1}).[60] The spectrum of PCL-PANI fibers also shows the characteristic peaks corresponding to the benzenoid (799 cm^{-1}) and quinoid (1566 cm^{-1}) groups of PANI. The spectrum of PGS, as synthesized, raw material shows the characteristic peaks previously described,[65,66] namely peaks corresponding to the ester groups established between sebacic acid and glycerol (1037 cm^{-1}, 1092 cm^{-1} and 1160 cm^{-1}), a blunt peak for the carbonyl groups (1725 cm^{-1}) and a broad peak (centered at 3451 cm^{-1}) corresponding to free unreacted hydroxyl groups. Finally, the spectrum of PGS/PCL-PANI fibers has peaks common to both PCL-PANI fibers and PGS raw material and shows no new peaks. This suggests that PGS and PCL-PANI are two discrete chemical entities inside the resulting coaxial fibers (core and shell, respectively).

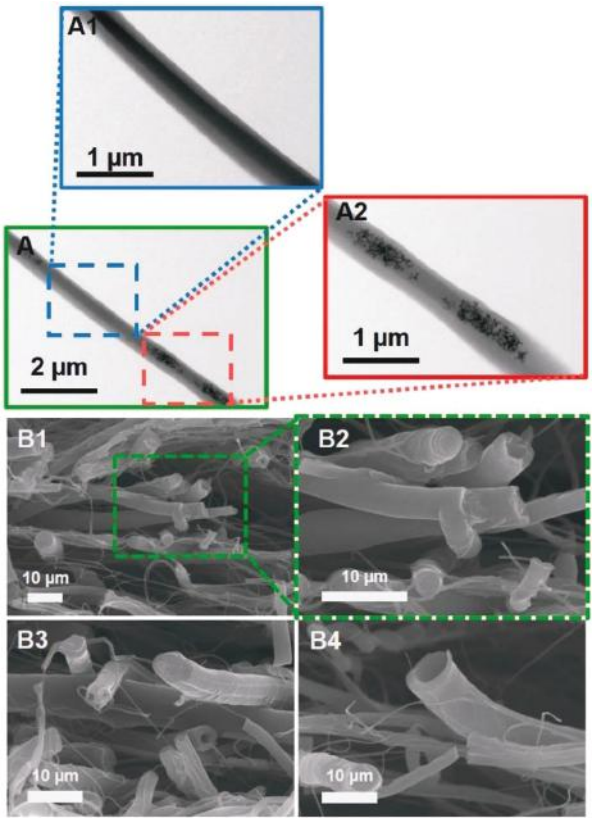

Fig. 2 (A) TEM image of a PGS/PCL-PANI fibers and magnification of two different areas (A1 and A2), using colloidal TiO_2 as the contrast. (B1–4) SEM images of PGS/PCL-PANI coaxial fibers cross-sections.

The phase separation between the two layers of the coaxial fibers was confirmed by DSC (Fig. 3B). Thermograms of the heating cycles are provided for PCL-PANI fibers (composite for the shell layer), PGS raw material (material for the core layer) and PGS/PCL-PANI fibers. The complete cycles are depicted in Fig. S1† and the corresponding transition temperatures and enthalpies are systematized in Table S3.† PCL-PANI fibers show a single major peak both in the heating (60.5 °C) and cooling (36.9 °C) cycles, ascribed to PCL.[60] PGS raw material shows two peaks in the heating cycles (4.1 °C and 17.7 °C) and a single peak in the cooling cycles (−13.4 °C), similar to what was described by Hou and colleagues.[59] The thermograms of PGS/PCL-PANI show the presence of both PCL-PANI and PGS

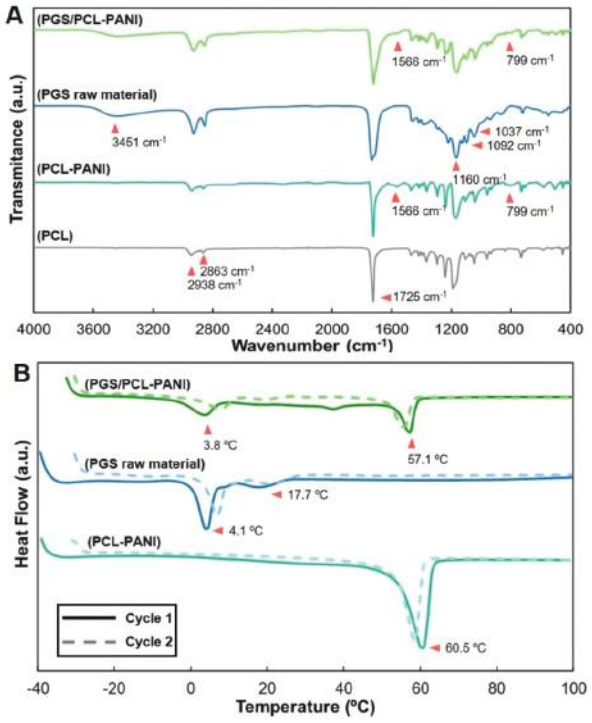

Fig. 3 (A) ATR-FTIR Spectra for (top to bottom) PGS/PCL-PANI coaxial fibers, PGS raw material, PCL-PANI monoaxial fibers and PCL fibers. (B) Thermograms (heating cycles) of (top to bottom) PGS/PCL-PANI coaxial fibers, PGS raw material and PCL-PANI monoaxial fibers.

peaks in both the heating (3.8 °C, and 57.1 °C) and cooling (28 °C and −5.3 °C) cycles. In the heating cycle when no melting of the materials had yet occurred the presence of these peaks and the unchanged enthalpies associated, suggest segregation between PCL-PANI (shell composite) and PGS (core material).[67,68] This confirms phase separation between the PGS core layer and the PCL-PANI shell layer, which is consistent with the coaxial structure of the fibers.

3.2. Critical properties for neural cell culture

We also evaluated other critical scaffolds properties for NSC culture under electrical stimulation. These properties include electroconductivity, mechanical properties surface properties, stability in PBS and degradability in lipase solutions. The main results, apart from stability, are summarized in Table 1.

3.2.1. Electroconductivity. Scaffolds with high values of electroconductive (> 10^{-2} S cm^{-1}) are reported to enable more efficiently cell maturation.[30,69–71] The electroconductivity values of monoaxial (PCL-PANI) and coaxial (PGS/PCL-PANI) fibers are very similar ($3.9 \pm 2.6 \times 10^{-2}$ S cm^{-1} *vs.* $6.3 \pm 2.9 \times 10^{-2}$ S cm^{-1} respectively). No statistically significant differences were found between the monoaxial and coaxial samples. Overall, the obtained coaxial fibers are electroconductive regardless their structure.

3.2.2. Mechanical properties. The adequate mechanical properties of a scaffold can benefit neural biocompatibility.[72] The mechanical properties of the fibers are shown in Fig. 4 The addition of PANI to PCL fibers lead to a statistically significant reduction in the Young modulus (7.0 ± 0.8 MPa to 2.0 ± 0.6 MPa), ultimate strength (2.2 ± 0.3 MPa to 0.3 ± 0.1 MPa) and maximum extension (180.8 ± 38.8% to 20.0 ± 6.3%). Surprisingly, this reduction in Young modulus (Fig. 4B and Table 1) conflicts to the results observed in our previous study, where an increase in stiffness was observed.[60] We believe this is caused by the presence of a more relaxed PANI : CSA chain, induced by the pseudo-doping properties of solvent system used for electrospinning and that was optimized in another study.[31] No differences were found between PGS/PCL-PANI coaxial and PCL-PANI monoaxial fibers in terms of Young modulus (1.3 ± 0.1 MPa), ultimate strength (0.2 ± 0.1 MPa) and maximum extension (21.1 ± 3.5%). This suggests the mechanical properties of the coaxial fibers to be determined mainly by the composition of the shell layer and not by both layers, which is consistent with the DSC and FTIR results. A similar phenomenon was observed in the work of Silva and colleagues,[58] but contrary to their work our coaxial fibers are softer and therefore better for neural tissue engineering applications.

3.2.3. Contact angle. The surface properties of scaffolds are important for neural cell adhesion and tissue biocompatibility.[73,74] The contact angle of the scaffolds was determined, using glycerol as the reference (Fig. S2†). The addition of PANI to PCL fibers promoted a decrease in the contact angle from 113 ± 8° to 65 ± 6°, probably due to the hydrophilic nature of PANI : CSA salt.[75] This decrease is statistically significant and shows that the surface of PCL-PANI fibers is now hydrophilic. Another decrease in the contact angle was observed for the coaxial fibers (38 ± 8°). This reduction of the contact angle of the PGS/PCL-PANI fiber mats, with respect to the PCL-PANI fibers, was taken as a possible PANI segregation at the surface of the coaxial fibers. It is likely

Table 1 Properties of PCL, PCL-PANI and PGS/PCL-PANI electrospun fibers

Sample	Fiber classification	Average diameter (nm)	Contact angle (Glycerol) (θ)	Young's modulus (MPa)	Electroconductivity (S cm^{-1})
PCL	Monoaxial	397 ± 235	113 ± 8	7.0 ± 0.8	—
PCL-PANI	Monoaxial	296 ± 93 (*)	65 ± 6 (*)	2.0 ± 0.6 (*)	$3.9 \pm 2.6 \times 10^{-2}$
PGS/PCL-PANI	Coaxial	951 ± 465 (*) (+)	38 ± 8 (*) (+)	1.3 ± 0.1 (*)	$6.3 \pm 2.9 \times 10^{-2}$

(*) mean $p < 0.05$ to PCL; (+) mean $p < 0.05$ to PCL-PANI; fiber diameter $n = 100$; contact angle $n = 6$; Young modulus $n = 6$; electroconductivity $n = 3$.

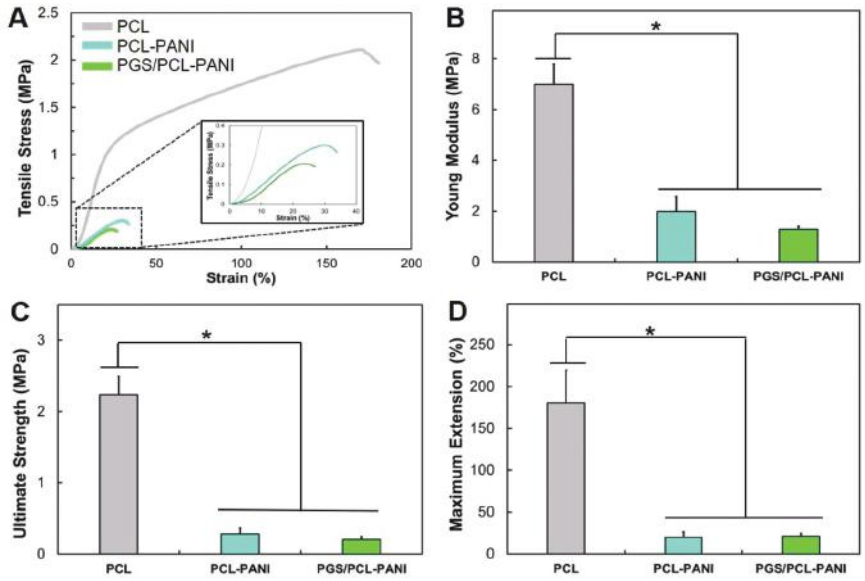

Fig. 4 Mechanical properties of PCL, PCL-PANI and PGS/PCL-PANI fibers: (A) stress–strain curves for the samples tested; (B) Young's tensile modulus, (C) ultimate strength and (D) maximum extension (* means $p < 0.05$) (mean ± std, $n = 6$).

that this segregation may lead to a higher conductivity. It is also possible that HFP released during electrospinning may interact with PANI and affect its conductivity by a pseudo-doping effect.[76] This would lead to PANI chain relaxation, increasing the number of contact points between different PANI chains and improve the mat's conductivity.

3.2.4. Fiber biodegradability in lipase solution and stability in PBS

Lipase degradation assay. Lipase (0.5 U mL^{-1}) was used as a model for cell-induced degradation of our substrate, mimicking the presence of cells on the fibers. The timepoints chosen for the assay were short (1 h, 4 h, 8 h, 12 h, 24 h, 48 h and 168 h) due to fast substrate degradation. Both the images of the fibers throughout the timepoints tested (Fig. 5A and S3†) and the respective FTIR profiles (Fig. S4†) evidence a heterogeneous degradation pattern for all the samples.

Starting with PCL fibers, their FTIR profile does not show significant changes in the chemical profile until the end of the assay. The supernatant pH initially decreases (hour 1 – 6.9) (hour 4 – 5.1), after which it remains constant (hour 24 – 4.3) (hour 168 – 4.0). Water content remains stable until hour 8 (78.9) before decreasing until complete degradation. SEM images indicate fiber diameter increased to 1035 ± 315 nm after 1 hour of incubation (Table S4†). Fiber diameter and morphology remained relatively constant until complete degradation of the fibers (12 h).

For PCL-PANI fibers, the FTIR profile (Fig. S4B†) shows an increased intensity of the characteristic PANI : CSA aromatic peaks (810 cm^{-1} and 1567 cm^{-1}), aromatic amines (1297 cm^{-1}) and amine salts (1477 cm^{-1}), suggesting a preferential degradation of PCL by the lipase. Degradation (mass remaining of 53.9% at hour 168) was not complete in the experimental time-frame (Fig. 5B). Water content was constant (87.0% at hour 168) and the supernatant pH slowly decreased from hour 1 (7.0) to hour 168 (6.5). Finally, fiber diameter increased initially to 581 ± 281 nm (1 h of incubation) and then to 994 ± 491 nm only 24 h after the start of the assay, remaining constant until the end of the assay (168 h).

The FTIR profile of PGS/PCL-PANI fibers (Fig. S4C†) evidence changes in the fingerprint region (800–1400 cm^{-1}) to resemble that of PCL-PANI fibers. SEM images of PGS/PCL-PANI fibers at timepoint 168h (Fig. 5A and S3†) do not evidence structural changes, except for core layer degradation visible at hour 168 (see red arrows in Fig. 5A). Mass remaining (Fig. 5B) decreased at hour 1 (53.7%), associated to both solvent loss and substrate degradation, and then slowly decreased until hour 168 (28.4%). Water content of PGS/PCL-PANI fibers slightly increases from hour 1 (81.7%) to hour 168 (89.6%) and the supernatant's pH remains low until the end of the assay (hour 168 – 4.8). Fiber co-axial diameter also increased at the start of the assay (1489 ± 696 nm at 1 h) and then again at hour 12 (1728 ± 870), remaining constant until the end of the assay at hour 168 (1704 ± 811). Finally, electroconductivity of PGS/PCL-PANI fibers was evaluated for timepoints 0 h ($6.3 \pm 2.9 \times 10^{-2}$ S cm^{-1}), 24 h ($(1.1 \pm 0.3) \times 10^{-3}$ S cm^{-1}) and 168 h ($(1.5 \pm 0.9) \times 10^{-4}$ S cm^{-1}). These values indicate that lipase can negatively impact the electroconductivity of PGS/PCL-PANI fibers. To better understand these changes, we performed a stability assay with only PBS.

PBS stability assay. While biodegradation is important for tissue engineering *in vivo* applications, scaffold stability is important for preparation of samples and *in vitro* cells culture. PBS solution was used as a control for inducing physico-chemical changes the fibers would suffer in cell-like con-

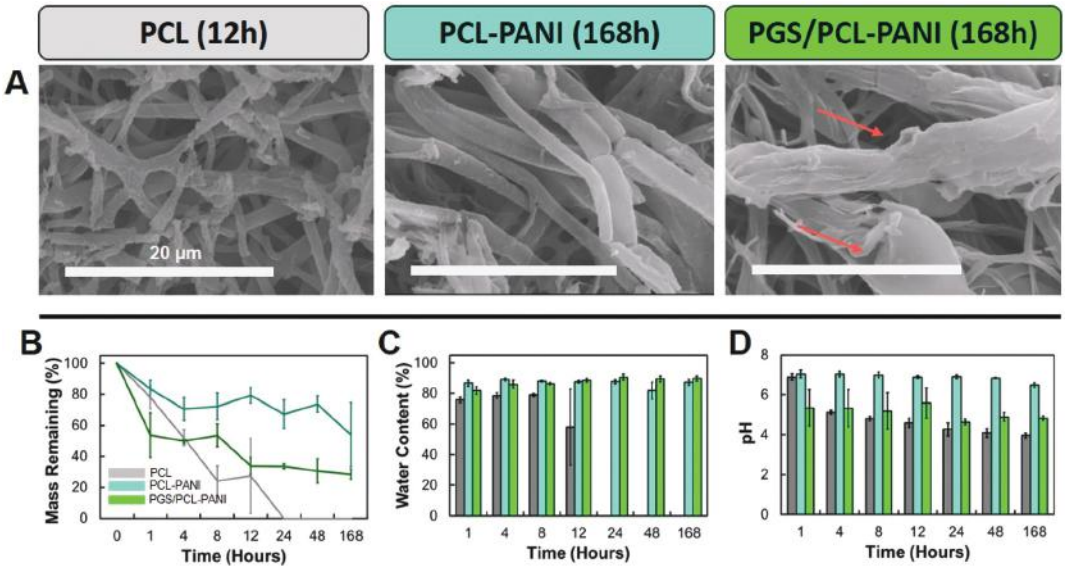

Fig. 5 Evaluation of the stability of the electrospun samples, performed with Lipase (0.5 U mL^{-1}) from *Aspergillus oryzae* (37 °C and 5% CO_2). (A) SEM images of fibers obtained at the last timepoint collected (hollow structures identified by red arrows). (B) Mass remaining (%) of the different samples tested and (C) water content of the corresponding fiber samples. Complementary evaluation of the (D) pH of the supernatants (mean ± std, $n = 3$).

ditions, with timepoints selected to match an *in vitro* cell culture experiments (days 4, 7, 14, 21 and 28).

SEM images of PCL fibers (Fig. 6A) do not evidence structural changes in the fiber mat. FTIR profile (Fig. S5A†) and mass remaining (Fig. 6B) (99.5% at day 28) do not evidence significant chemical and/or mass changes. The supernatant's pH (7.2 at day 28) (Fig. 6C) and water content (39.1% at day 28) (Fig. 6D) do not change significantly until the end of the assay. Fiber diameter (Table S5†) increases at day 4 (891 ± 344) and remains stable until the end of the assay at day 28 (879 ± 266).

For PCL-PANI fibers, no significant changes in fiber visual aspect (Fig. 6A) and chemistry (Fig. S5B†) were observed. It was observed an increase in fiber diameter (Table S5†) at day 4 (671 ± 309) but no significant changes after until day 28 (747 ± 418). Mass remaining (Fig. 6B) slightly decreases at day 4 (88.6%) and remains constant until day 28 (89.7%) and is likely attributed to CSA leaching and residual solvent loss. The supernatant pH (Fig. 6C) remains constant (7.1 at day 28), and water content (Fig. 6D) slightly increases until the end of the assay (85.0 at day 28). The obtained samples were not electroconductive (Fig. 6E).

For PGS/PCL-PANI fibers, no significant changes in the fibers visual aspect (Fig. 6A) nor their chemical profile (Fig. S5C†) were observed. Fiber diameter (Table S5†) also increased at day 4 (2400 ± 1733) and remain relatively constant until the end of the assay at day 28 (2595 ± 1887). Overall remaining mass (Fig. 6B) decreases at day 4 (70.7%) and again at day 7 (62.9%) before stabilizing until day 28 (64.1%), attributed to the release of entrapped solvent or low molecular weight PGS from the core layer. In fact, the pH of the supernatant (Fig. 6C) decreases at day 4 (5.1) and remains constant until the end (5.7 at day 28) due to the acidic products released. Water content (Fig. 6C) remains constant (83.6 at day 28). Electroconductivity was measured for all timepoints (Fig. 6D): for day 4 of 5.7×10^{-3} S cm^{-1}, for day 7 of 3.2×10^{-2} S cm^{-1}, for day 14 of 1.1×10^{-2} S cm^{-1}, for day 21 of 1.3×10^{-3} S cm^{-1} and finally for day 28 of 1.9×10^{-4} S cm^{-1}. No statistically significant differences were found between any of the samples. As such, electroconductivity was found to be constant up to days 14-21, with a slight decrease observed at day 28. Contrary to the lipase assay, no degradation of the core layer was identified visually or by FTIR, suggesting a potential role of it in electroconductivity stabilization.

In summary, we determined the *in vitro* behavior of PGS/PCL-PANI fibers in PBS and a lipase solution. With PBS, we showed that the coaxial fibers are stable and their electroconductivity remains constant for up to 21 days, with a 10-fold decrease observed at day 28. With lipase solution, we showed that biodegradation of PGS/PCL-PANI fibers still occurs under cell culture conditions and the shell layer, responsible for cell support, is more stable. We then proceeded to evaluate the performance of these fibers for future neural tissue engineering applications, using neural-differentiating iPSCs.

3.3. Induced pluripotent stem cell (iPSC) culture and initial neural differentiation

iPSCs hold promise in the design of reliable *in* vitro models to study disease progression and test drugs, and also for future applications in transplant. As such, iPSCs were chosen as the

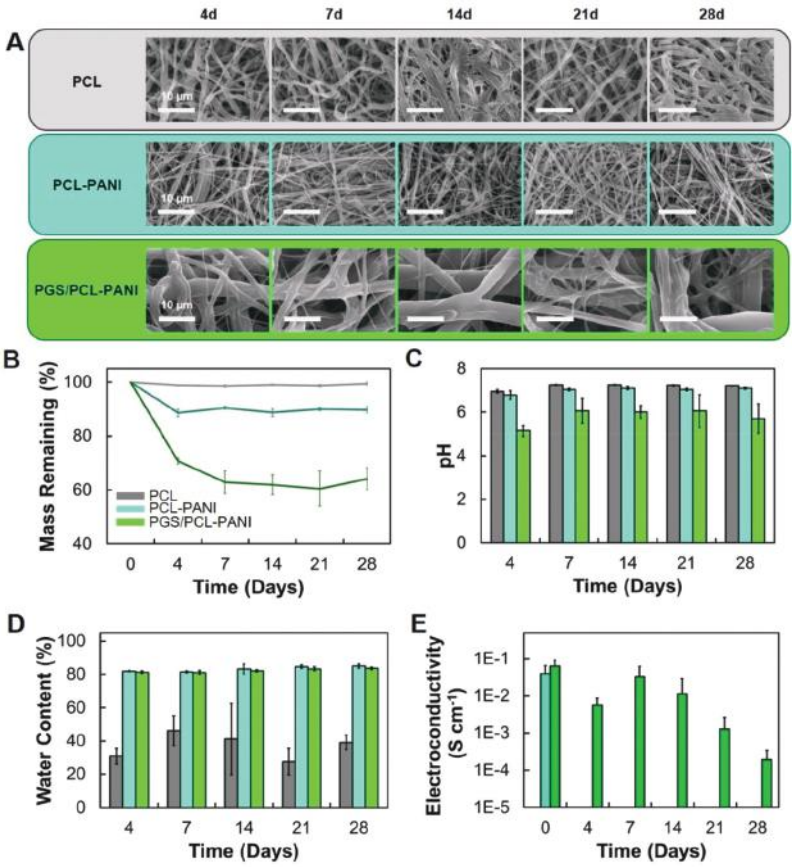

Fig. 6 Evaluation of the stability of the electrospun samples in PBS. (A) SEM images of fibers obtained at different timepoints. (B) Mass remaining (%) of the different samples tested, (C) pH of the supernatants, (D) water content and (E) electroconductivity of the corresponding fiber samples were also evaluated (mean ± std, n = 3).

best cell model to study the applicability of our coaxial scaffold to neural tissue engineering applications. The first step on using iPSCs for cell culture was to confirm their pluripotency at day 0 of differentiation. We found the presence of pluripotency markers such as the transcription factors OCT4 (94.4 ± 6.4%) and SOX2 (91.0 ± 6.7%) (Fig. 7A1-2, 7E and S6B†) by both IF and FC, and the membrane markers TRA-1-60 and SSEA-4 (Fig. 7A3-4 and S6A†) by IF. Overall, the iPSCs used were found to be pluripotent.

In the next step we promoted the neural differentiation of iPSCs following the protocol of Fernandes and colleagues[23] (Fig. 8B) and monitored the efficiency of the neural induction protocol. Differentiated cells showed the desired neural phenotype at days 12 and 17, which was evaluated by immunofluorescence (IF) (Fig. 7B-C), flow cytometry (FC) (Fig. 7D and S6B-D†) and qPCR (Fig. 7E). Fernandes and colleagues reported a drastic reduction in OCT4 expression and the presence of a neuroepithelial layer by day 12 of differentiation.[23] By FC, we observed that at days 12 and 17 of neural differentiation the percentage of OCT4+ cells (10.3 ± 2.2% and 9.3 ± 6.2% respectively) was significantly lower than at day 0, but no significant changes were observed for SOX2 at days 12 (85.8 ± 10.3%) and 17 (94.6 ± 1.7%) (Fig. 7E). By IF we observed NES+/PAX6+cells at day 12 (Fig. 7B) and NES+/ZO1+ cells grouped in neural rosettes at day 17 (Fig. 7C).

We also confirmed neural commitment of the cells by using qPCR analysis (Fig. 7E). There is no change in the expression of the NSC markers SOX2 and NES at days 12 and 17. For PAX6, TBR2 and TBR1, all early-neural differentiation markers, expression increases at days 12 and 17. At day 12, PAX6 levels are at the highest, followed by TBR2 and TBR1, and at day 17 PAX6 level decrease whereas those of TBR1 and TBR2 rise. Englund and colleagues[77] reported that these three markers are sequentially expressed *in vivo* in the developing neocortex of mice. Along with this variation, we observe an increase in the expression of TUBB3, DCX and NCAM at both days 12 and 17. All these results indicate neural differentiation is progressing normally and cells progressed from iPSCs to iNPCs, with potential to differentiate into cortical neurons. We therefore decided to seed the iNPCs (neural rosettes) obtained at day 17 on our electrospun scaffolds to compare the performance of the fibers obtained on neural differentiation.

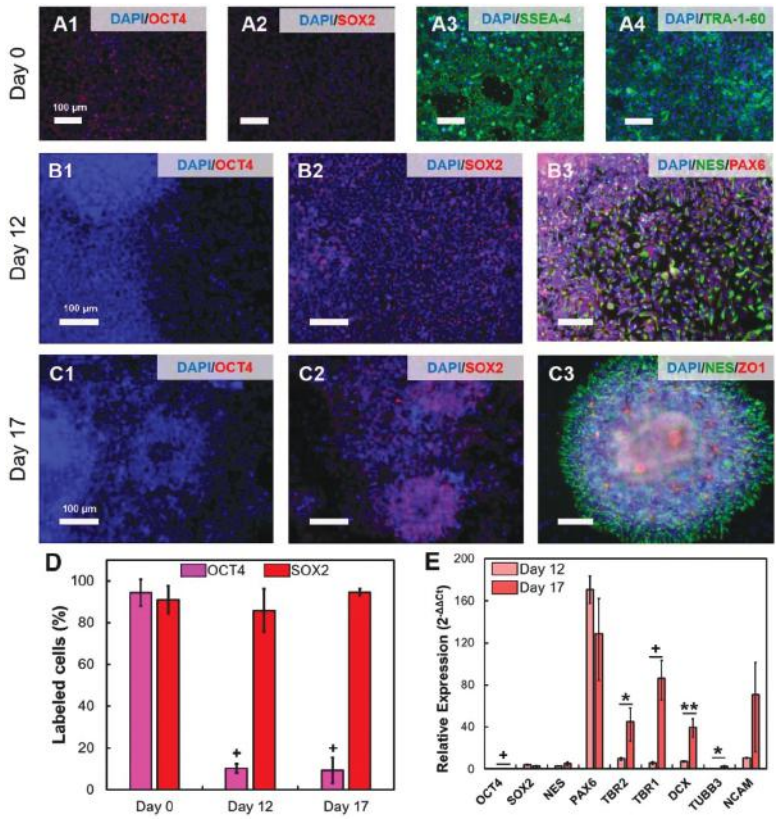

Fig. 7 (A1–4) Immunofluorescence of undifferentiated iPSCs and respective pluripotency markers OCT4 (A1) and SOX2 (A2), both intracellular, and TRA-1-60 (A3) and SSEA-4 (A4), both extracellular. Differentiation was evaluated for OCT4 and SOX2 at days 12 (B1-2) and 17 (C1-2). Complementary staining for other neural markers was also performed at days 12 (C3 – NES and PAX6) and 17 (D3 – NES and ZO1). The quantification of FC markers fluorescence intensity for OCT4 and SOX2 was performed (D) ((+) means $p < 0.001$ compared to day 0, $n = 4$). qPCR analysis of iPSCs (E) differentiating for 17 days on adherent plates for the genes OCT4 (pluripotency), SOX2 (pluripotency and NSCs), NES (early NSs), PAX6 (radial glia), TBR2 (intermediate progenitor cells), TBR1 (post-mitotic neurons), DCX (early neurons), TUBB3 (early neurons) and NCAM (intermediate neurons) (mean ± SEM; $n = 3$; (*) means $p < 0.05$, (**) means $p < 0.01$, (+) means $p < 0.001$).

3.4. iNPC differentiation on electrospun scaffolds

In a first approach, the iNPCs obtained after 17 days of iPSCs differentiation were seeded on the fibers prepared in this study and left to differentiate in plain N2B27 medium for 30 days (47 days in total). Cell neural differentiation was evaluated through the analysis of cell morphology and neural marker expression. SEM imaging of differentiated cells on PCL, PCL-PANI and PGS/PCL-PANI fibers (Fig. 9A–C) show that cells were able to attach and spread on all scaffolds tested. Subsequent IF analysis shows that these cells were neurons (Tuj1+) (Fig. 9D–F), similar to the ones differentiated on regular culture plates (Fig. S6†), that present long neurites with random orientation (MAP2+) (Fig. 9G–I) and are capable of producing synaptic vesicles (SYP+) (Fig. 9J–L). The morphology of the obtained neurons was similar, independently of the scaffold used as a support, for the several cell cultures. The randomly-oriented neurites are seen to interact with other neurites, cell bodies and the fibers themselves forming "neural-network" structures that denote the biocompatible profile of all the fibers tested.

The literature is not consistent about the more adequate differentiation marker(s) for qPCR, using our differentiation protocol. As such, several neural markers (Fig. 10 and S9†) from different neural differentiation stages were selected and tested. The expression of the early iNPC marker (NES) decreases until day 30 for all samples. The expression of early (DCX, TUBB3) and mature neural markers (MAP2, NCAM, NEUN) increases throughout the experiment for all samples. The expression of GABAergic neural marker GAD67 (GABAergic neurons), and dopaminergic markers (DRD2 and TH) also increases similarly for cell cultures on all fiber samples. No statistical differences were found between the different fibers tested.

The results obtained indicate that all fiber substrates can support neuron differentiation. Moreover, their maturation into GABAergic and dopaminergic lineages is not impaired, and that any of the neural markers selected can be used to

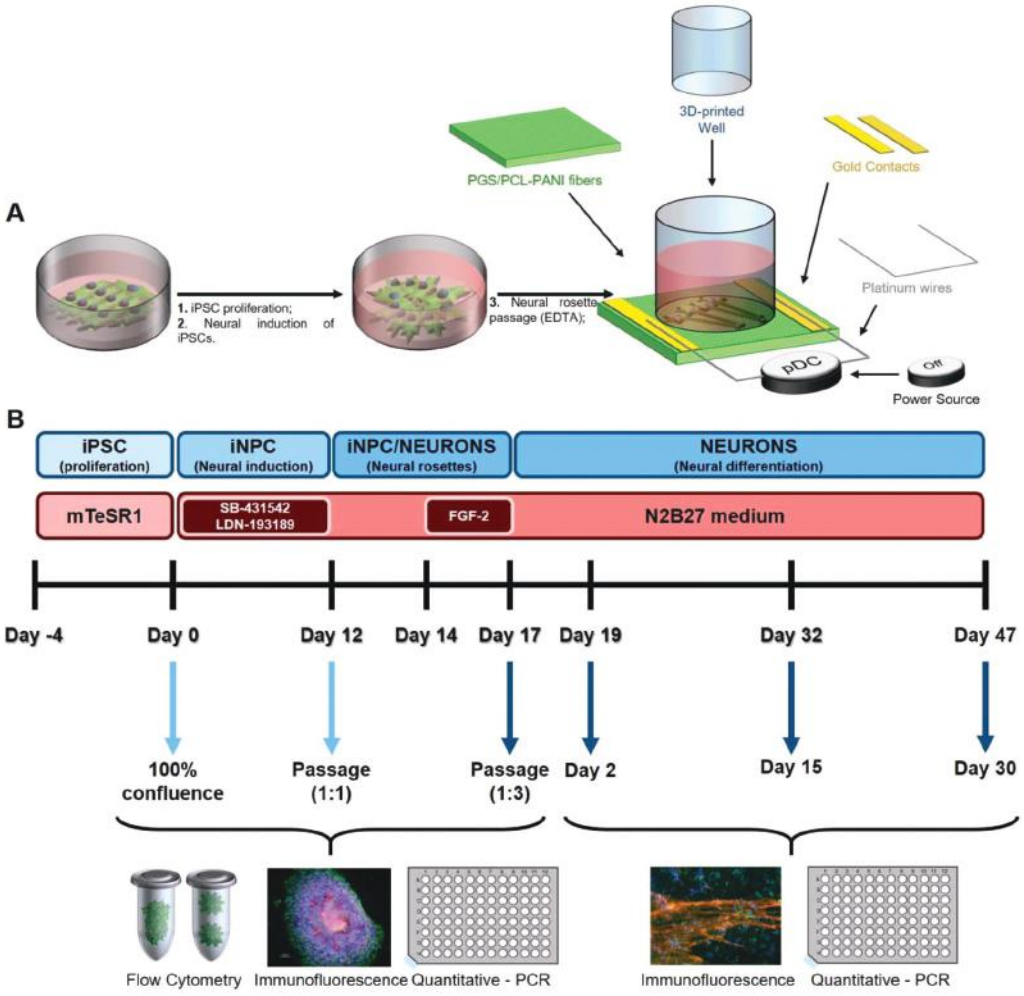

Fig. 8 (A) Overview of the components necessary for the assemblage of the electrical stimulation setup; (B) summary of the iPSC differentiation protocol into neurons used in this work.

monitor the progression of differentiating neurons using this protocol.

3.5. Electrical stimulation of differentiating iNPCs

The results obtained so far indicate that PGS/PCL-PANI fibers can support iNPC neural differentiation. Future biomedical applications of these fibers are numerous due to their favorable properties for neural tissue engineering, including the design of *in vitro* models to study disease progression and test drugs or even the production of more mature neurons to transplants into patients. In particular, electrical stimulation can be used to increase the effectiveness of tissue engineering based strategies for the neural applications by enhancing the differentiation of neural cells. As such, on a second set of studies, we decided to perform a pioneering attempt to investigate the effect of electrical stimulation on iPSC-derived differentiating neurons. We were particularly interested in understanding (1) the long-term effects of electrical stimulation (30 days) on differentiating iNPCs, and (2) whether electrical stimulation could benefit the differentiation of iNPCs into lineage-specific neurons such as glutamatergic, GABAergic and dopaminergic ones.

The devised strategy used for culturing and differentiating iNPCs under electrical stimulation on PGS/PCL-PANI fibers is depicted in Fig. 8A (Assemblage of the electrical stimulation setup) and Fig. 8B (General protocol for the neural differentiation of iPSCs). Based on previous work of our group,[28,29,31] we decided to use a pulsatile DC regimen (1 V cm^{-1}, 100 Hz) throughout 30 days of cell culture (day 17–day 47). The main results obtained are presented in Fig. 11 and 12.

Electrical stimulation induced morphological changes on the cells. As it can be seen by the SEM images, the non-stimulated cells have their cell bodies and neurites/axons distributed randomly (Fig. 11A). The stimulated cells are organized into fiber-like bundles with aligned neurites/axons (Fig. 11B), and "cell-body" clusters can occasionally be detected at one end of

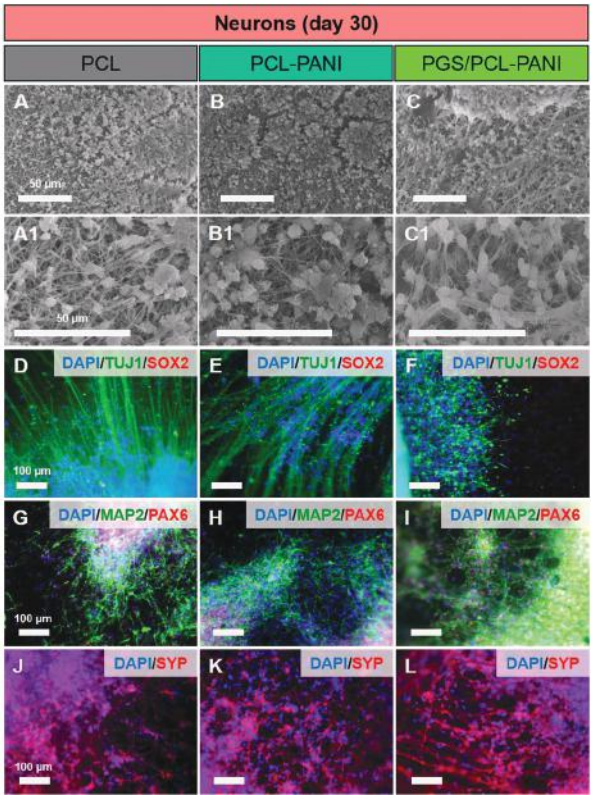

Fig. 9 Morphological analysis and marker expression of iNPCs differentiated for 30 days on PCL, PCL-PANI and PGS/PCL-PANI fibers. SEM images, at various magnifications, (A–C). IF images for neural marker expression: Tuj1 (D–F), Map2 and Pax6 (G–I), and Syn (J–L), with DAPI as the counter-stain.

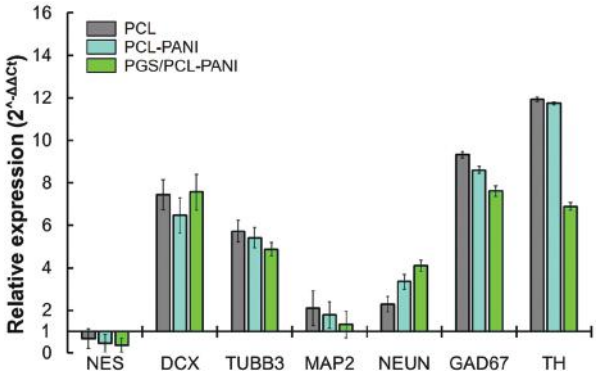

Fig. 10 Overall neural markers profile of neurons after 30 days of differentiation on the electrospun fibers by qPCR analysis (ΔΔCt method and relative to cell on day 17): NES (neural progenitor cells), DCX and TUBB3 (neurons – early markers), MAP2 and NEUN (neurons – mature markers), GAD67 (GABAergic neurons), and TH (dopaminergic neurons). (mean ± sem, n = 3).

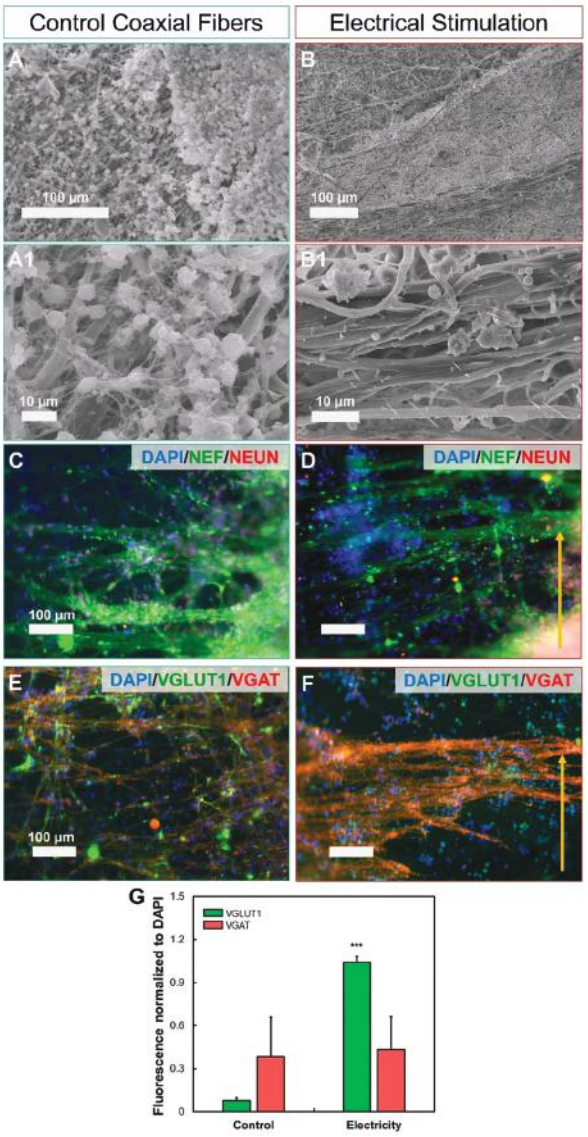

Fig. 11 SEM images of neurons differentiated for 30 days on PGS/PCL-PANI fibers, without (A,A1) or with electrical stimulation (B,B1). Respective IF images were also obtained, including NEF and NEUN without (C) or with electrical stimulation (D); and VGLUT1 and VGAT without (E) or with electrical stimulation (F). Additionally, VGLUT and VGAT fluorescence intensities were quantified (G) (mean ± std, n = 5, (***) means $p < 0.005$).

the bundles (Fig. S10†). IF staining with NEF/NEUN (Fig. 11C and D) confirmed the cells present in the scaffolds at day 30 were neurons. When VGAT/VGLUT1 staining was performed, we observed the coexistence of VGAT+/VGLUT1− with VGAT−/VGLUT1+ neurons in the cell population not exposed to electrical stimulation. However, in the electrically stimulated cultures there is a predominance of VGAT+/VGLUT1+ cells. We performed a complementary analysis on fluorescence intensity of VGAT and VGLUT1 on both samples and found statistically significant higher VGLUT1 values in the electrical stimulated samples.

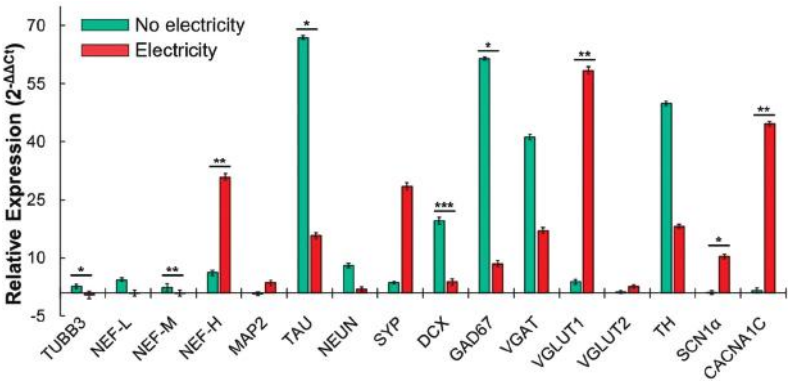

Fig. 12 The mRNA expression of genes for early neurons (DCX, TUBB3), intermediate neurons (MAP2, NEUN), mature neurons (NEF-L, NEF-M, NEF-H, TAU, SYP), GABAergic neurons (VGAT, GAD67), glutamatergic neurons (VGLUT1, VGLUT2), dopaminergic neurons (TH) and voltage-sensitive channels present in matured neurons (SCN1α and CACNA1C) were evaluated to monitor the different maturation stages of the cells. (mean ± sem, n = 3, (*) means $p < 0.05$, (**) means $p < 0.01$, (***) means $p < 0.005$).

The cells obtained were further analyzed by qPCR (Fig. 12). Significant changes in the expression of different neural markers were observed after electrical stimulation was applied. There were changes in the expression of neural differentiation markers associated with the cytoskeleton, including a decrease in TUBB3 (0.18-fold – statistically significant), NEF-L (0.21-fold), NEF-M (0.39-fold – statistically significant), DCX (0.19-fold – statistically significant) and TAU (0.24-fold – statistically significant) and an increase in NEF-H (4.97-fold – statistically significant) and MAP2 (4.96-fold). MAP2, TAU and DCX are microtubule-associated proteins, able to stabilize the intracellular tubulin filaments. In mature non-migratory neurons DCX expression is greatly reduced, and therefore a reduction in its mRNA levels indicates maturation.[78] MAP2 co-localizes on neurites and TAU on axons,[79] and therefore changes in their expression can suggest dynamism in neurite/axon formation. The expression levels of TUBB3 and NEF-H are inverse and might indicate the formation of mature axons with higher caliber.[80]

The levels of other neural markers also changed. We observed a decrease in mRNA levels of the splicing factor NEUN (0.25-fold), and of the adhesion molecule NCAM (0.56-fold), but an increase in the levels of SYP (7.80-fold – statistically significant), SCN1α (12.73-fold – statistically significant) and CACNA1C (32.13-fold – statistically significant). SYP is a protein associated with synaptic vesicles and therefore is an indirect indicator of synapse formation. An increase in SYP expression might indicate the formation of more synapses between adjacent neurons and the establishment of a neural network, a sign of neural maturation.[81] SYP upregulation is also accompanied by increased mRNA expression of CACNA1C (voltage-dependent calcium channel component) and SCN1α (voltage-dependent sodium channel component). This also confirms the presence of more mature and functionally active neurons, able to express components involved in synaptic signal transduction.[82]

To obtain a more complete maturation profile of the obtained neurons, we analyzed more specific lineage markers such as GAD67 and VGAT (GABAergic neurons), VGLUT1 and VGLUT2 (glutamatergic neurons), and TH and DRD2 (dopaminergic neurons). We found after electrical stimulation a decrease in the mRNA levels of GAD67 (0.09-fold – statistically significant) and VGAT (0.42-fold), TH (0.39-fold) and DRD2 (0.15-fold). Conversely, we also observed an increase in the mRNA levels of VGLUT1 (14.55-fold – statistically significant) and VGLUT2 (3.20-fold). The dominance of one marker over the other usually determines if a neuron is excitatory (glutamatergic) or inhibitory (GABAergic). Overall, these data show a switch towards excitatory, glutamatergic profile of neurons upon electrical stimulation, with concomitant decrease in GABAergic and dopaminergic markers. Interestingly, the above mentioned decrease in DCX expression points out to the same trend, as DCX is expressed mostly in GABAergic interneurons that are generated in ganglionic eminences and undergo migration to the cortex where they integrate functional circuits.[83]

4. Discussion

Our work reports for the first time the production of electroconductive and biodegradable coaxial fibers composed of a PCL-PANI outer shell, whose electroconductivity is enhanced through the use of the solvent system TFE : HFP 5 : 5, and an inner core composed of PGS. PGS/PCL-PANI fibers can direct electrical current to cells cultured on top and therefore have potential applications in neural tissue engineering. In a first stage, the fibers used in this work were electrospun using the solutions described in Table S1† and the setups depicted in Fig. 1A and 2B. PGS/PCL-PANI fibers are the coaxial fibers envisaged for neural tissue engineering applications, whether PCL-PANI and PCL fibers are controls for the several studies

developed here. All fibers were characterized regarding their morphology and physico-chemical properties in order to understand the behavior of the materials used in our system. The techniques used allowed to directly (SEM, TEM) and indirectly (FTIR, DSC, mechanical properties) prove the existence of a coaxial structure on PGS/PCL-PANI fibers.

The obtained coaxial PGS/PCL-PANI fibers have an average diameter of 951 ± 465 nm. Previous studies reported the positive effects of fiber diameter on neural cells culture. Christopherson and colleagues reported that large diameter fibers promote neural differentiation.[84] Wang and colleagues reported that large diameter fibers promote Schwan cell migration.[85] Finally, Johnson and colleagues reported that large diameter fibers (808 nm) can promote astrocyte elongation and neurite outgrowth.[86] As was reported by Ankam and colleagues[87,88] and Yang and colleagues,[30] these positive effects can be justified by the production of tension on the cytoskeleton and induce actomyosin contractibility, leading to improved cell differentiation. We therefore expect the higher diameter of our coaxial PGS/PCL-PANI fibers to be favorable for neural differentiation of iPSCs.

Mechanical properties are important to maximize the biocompatibility of biomaterials. For neural tissue engineering applications, a scaffold should have a Young's (elastic) modulus closer to that the brain tissue, around 0.1–10 kPa.[89,90] However, electrospun fibers typically have Young's modulus values in the MPa range (>0.4 MPa), and its magnitude depends on the materials and production strategies used.[91,92] As such, any significant decrease will greatly benefit the future applications of electrospun scaffolds in neural tissue engineering. Our PGS/PCL-PANI coaxial fibers have a Young's modulus of 1.3 ± 0.2 MPa, lower than the PGS/PCL fibers produced by Silva and colleagues[58] (5.1 ± 1.5 MPa) containing a shell layer with less PCL. Such reduction was due to the strategy used for the production of our shell layer, composed of PCL-PANI dispersed in a solvent system containing equal amounts of TFE and HFP. This solvent system was optimized in our previous work[31] to enhance both the electroconductive and mechanical properties of PCL-PANI fibers due to a pseudo-doping induced relaxation of PANI : CSA chains. In fact, such effect is responsible for the reduction in Young's modulus of PCL-PANI fibers (2.0 ± 0.6 MPa) vs PCL fibers (7.0 ± 0.8 MPa) produced in this work.

The assessment of our PGS/PCL-PANI fibers *in vitro* performance in culture-like conditions is also an important step to evaluate its applicability on neural tissue engineering. In particular, biodegradability in the presence of an enzyme is especially important for scaffold applicability in neural culture, as the ability of NSCs to remodel their substrate can influence their stemness and differentiation efficiency.[38,39]

The selection of lipase for the biodegradation study was not random. The brain tissue is rich in enzymatic activity,[93,94] and particularly in lipoprotein lipases, a specific subtype of triacylglycerol lipases that can cleave carboxylic ester-bonds of water insoluble triacylglycerols.[95] They are naturally present at the surface of cells, including neurons and astrocytes where they are involved in metabolic balance and lipid homeostasis.[96,97] Since lipases are the most capable of degrading both PCL and PGS, they can impact the potential performance of our scaffold and are therefore our choice to study the performance of the coaxial fibers.

Fiber degradation induced by lipase was not homogeneous for all the samples tested. While in PCL fibers degradation was homogeneous and fibers disappeared after 24 h, by the end of the assay about 67.1% of PCL-PANI and 33.5% of PGS/PCL-PANI fibers mass remained. In the case of PCL-PANI fibers, we hypothesize that PANI : CSA might prevent PCL degradation by direct adsorption of the lipase.[98,99] This might also explain why the core-layer is preferentially degraded (see red arrows in Fig. 5A) by lipase whereas the shell layer is not. This can be attributed to the absorption of solution by the fibers, as was suggested by the high fiber diameters and water intake values observed at the various experimental timepoints.

Fiber composition is the following: PCL-PANI fibers, 89% of PCL and 11% of PANI : CSA; PGS/PCL-PANI fibers, 43% of PGS, 51% of PCL and 6% of PANI : CSA. The results on the accelerate human lipase degradation assay clearly show that PCL-PANI and PGS/PCL-PANI fibers are biodegradable, an important feature for neural tissue remodeling. Still, their weight loss in this assay, shows a degradation rate slower than for PCL fibers and final values above to the one that can be allocated to PANI alone.

While fiber degradation with lipase is important for cell applications, the evaluation of their physico-chemical stability in culture-like conditions and using a chemically defined medium (PBS) allows us to evaluate their long-term performance. The PBS stability results evidence a major improvement in the electroconductivity stability of the coaxial fibers, in an extent not observed in other studies. For example, in the study of Qazi and colleagues[65] the performance of different PGS-PANI blends was evaluated. In there, the cross-linking (120 °C for 24 h) of PGS pre-polymer blended with PANI : CSA was maximized to increase hydrophobicity, leading to a reduction in CSA leaching and improving the stability of PANI : CSA. The best sample tested (PGS-PANI 30%) had an electroconductivity of 1.77×10^{-2} S cm^{-1}, which decreased to 1.03×10^{-3} S cm^{-1} (0.1 fold) after 4 days in PBS. In our study the coaxial fibers (6.3×10^{-2} S cm^{-1}) are able to maintain their electroconductivity constant up to 21 days (1.3×10^{-3} S cm^{-1}). A slight reduction in electroconductivity is observed at day 28 and indicates the presence of electroconductive PANI : CSA inside the fibers. Moreover, the shell layer of our PGS/PCL-PANI fibers is composed of 10% of PANI : CSA dispersed in PCL, opposed to 30% in PGS composite studied by Qazi and colleagues. Contrary to the lipase stability assay, the PGS core layer was not compromised throughout the PBS assay. We hypothesize that the same PGS layer might provide a slightly acidic microenvironment, inside the fibers, that promotes PANI : CSA stability and retards doping and electroconductivity loss. Nevertheless, further studies are necessary to understand the mechanism behind this improved performance.

The water content and average fiber diameter of PGS/PCL-PANI fibers is high throughout each one of the degradability and stability assays, a consequence of the hydrophilic nature of PANI[75] In PBS, our PGS/PCL-PANI fibers have a water content of 83.6% at day 28. When in lipase solution, the water content increases to 89.6% at hour 168 (1 week). Moreover, the values for fiber diameter were more stable during the PBS assay than throughout the lipase assay. It is possible that the consequent lipase-driven PCL and/or PGS degradation might render the fibers increasing hydrophilic, which increases their ability to entrap water and forces the fibers to swell. From a scaffold point of view, the high water content found in PGS/PCL-PANI fibers is excellent for neural tissue engineering applications. The only systems containing more water are hydrogels, which are composed by high water-absorbable polymeric materials that enable water contents ranging between 92% and 99.5%.[100,101] Nevertheless, the high water content value found indicates that the fiber mats have the potential to ease the transport of nutrients and oxygen to the cultured cells and cell migration inside the scaffold. For our coaxial fibers, such feature, associated with an interesting Young's modulus (1.3 ± 0.2 MPa) and electroconductivity (6.3 ± 2.9 × 10^{-2} S cm^{-1}), make these fibers promising candidates for neural tissue engineering applications.

The next step in our work was to differentiate iNPCs from iPSCs. This can achieved by means of well-established protocols, such as the dual SMAD inhibition one.[16,23,61] A modified version of this protocol was performed for neural induction, and it is summarized in Fig. 8B. Some important hallmarks include the establishment of functional synapses after 40-50 days and the appearance of functional cortical networks, composed by VGLU1+ neurons (glutamatergic), 60–90 days after neural induction.[16,23] In this protocol, efficient neural differentiation of iPSCs into PAX6+ induced neural progenitor cells (iNPCs) is achieved by using activin/nodal pathway inhibitor SB-431542 and the BMP pathway inhibitor LDN-193189, leading to the suppression of both mesoderm and trophectoderm differentiation (dual SMAD inhibition). Our results show that neural differentiation progresses normally and according to the expected outcomes (Fig. 7 and S6†).

The dual SMAD inhibition protocol used in this work for neural differentiation was adapted from Fernandes and colleagues,[23] and chosen due to its versatility and capacity to yield a wide variety of neurons, including cortical glutamatergic (VGLUT1+) by differentiation day 120. However, it is expected that these and other types of neurons, including GABAergic and Dopaminergic, can also be detected in culture at varying amounts earlier in the differentiation process. In the work of Rhee and colleagues,[102] a similar protocol, though using 5 times more concentrated SB and LDN in the media, was used to obtain mature GABAergic neurons in a shorter period of 25 days of differentiation. Rhee and colleagues were also able to obtain mature glutamatergic (GLUT1+) neurons after 50 days of differentiation, using only the double the amount of LDN used here, but using a more complete supplemented culture media. In the pioneering work of Chambers and colleagues,[61] the dual SMAD inhibition strategy was used to generate dopaminergic (TH) and motor neurons.

We decided to evaluate the performance of the neural differentiation protocol on all the fibers produced here. Our results demonstrate that neural differentiation progresses normally (Fig. 9, 10, S8 and S9†), and at day 30 the population is composed by a mixture of VGAT+ (GABAergic) and VGLUT1+ (glutamatergic) neurons (Fig. 11). While the dopaminergic-neuron associated transcript TH was expressed by the neurons at days 15 and 30 (Fig. 10 and S9†), TH+ neurons could not be identified on the cells by IF. Moreover, in the absence of electrical stimulation, qPCR did not show any changes in GABAergic (GAD67) and dopaminergic marker (TH) expression on the cells cultivated on electroconductive fibers when compared to the ones cultivated with regular PCL fibers. While the sample size for the analysis (n = 3) might be underestimated, these results are intriguing and not completely in line with the literature available, as neural differentiation was expected to be enhanced in our electroconductive fibers (*e.g.* PCL-PANI and PGS/PCL-PANI). For example, Yang and colleagues[30] report an increase in GABAergic and dopaminergic neuron generation, based on IF, compared to glutamatergic, using embryonic stem cells cultured for 12 days on electroconductive substrates. In our work, at day 15 of differentiation (Fig. S8†) intricate networks of neurons (SYP+) are present in the neurons differentiated on both PCL-PANI and PGS/PCL-PANI substrates. Moreover, neural rosettes are still detected in both PCL and PCL-PANI fibers, whereas in PGS/PCL-PANI fibers they are absent. These observations suggest the existence of visually different neural maturation rates at day 15 for all the cells cultured on the different scaffolds, with PGS/PCL-PANI > PCL-PANI > PCL. These same differences are not supported by qPCR from day 15 samples (Fig. S9†) and such morphological differences are not perceived at day 30. We hypothesize that the beneficial effects of electroconductive substrates described by Yang and colleagues are due to an early acceleration of differentiation and/or an improvement neural cell migration/stretching caused by the electroconductive substrate.[11,103] Nevertheless, our substrates have different topography and a lower electroconductivity when compared to the titanium substrates used by Yang and colleagues (1250 S cm^{-1}). We believe further studies are necessary to fully evaluate the effect of electroconductive substrates on the enhancement of neural cell differentiation.

Electrical stimulation is a powerful tool capable of enhancing neural differentiation of NSCs (Table 2). Previous work from our group supports this hypothesis. Pires and colleagues observed a decrease in cell aspect ratio and an increased in the number of Tuj1+ (neurons) *vs.* Gfap (astrocytes) after AC electrical stimulation (1 V cm^{-1}) of human NSCs. Garrudo and colleagues observed a boost in the expression of both neural and astrocytic markers in differentiating NSCs after 4 days of AC electrical stimulation (1 V cm^{-1}), such as microtube associated protein 2 (MAP2), doublecortin (DCX) and S100 calcium-binding protein B (S100β). Yang and colleagues[30] observed that pulsed electrical stimulation (25 V, 3 μA) also enhanced

Table 2 Summary of NSC differentiation assays on electroconductive substrates under electrical stimulation

References	Cells used	Differentiation protocol	Substrate composition/type	Substrate electroconductivity	Electrical stimulation protocol	Neural cell profile
Garrudo and colleagues[31]	REN-VM cells (Passage 10)	N2B27 (4 days)	Electrospun monoaxial PCL-PANI 9% fibers	$1.9 \pm 0.4 \times 10^{-1}$ S cm^{-1}	AC, 1 V cm^{-1}, 100 Hz, 12 h on/12 h off.	Cell alignment with the direction of the electrical field. Boost in expression (qPCR) of MAP2 and S100β after electrical stimulation.
Oh and colleagues[107]	Human iPSCs (Passage 51–55)	1 – N2B27+ dual SMAD inhibition (Dorsomorphin (10^{-6} M) and SB431542 (10^{-6} M)) (7 days); 2 – N2B27+ 2-mercaptoethanol (10^{-4} M) + EGF (20 ng mL^{-1}) and bFGF (20 ng mL^{-1}) (8 or 14 days)	Conductive graphene scaffold (graphene oxide + carbon nanofibers)	$2.0–2.2 \times 10^{-3}$ S cm^{-1}	AC (±0.8 V), 100 Hz, 1 h at day 8	(Day 15) Increased generation (IF) of Tuj1+ and MAP2+ neurons after 7 days; (Day 15) Decreased expression (qPCR) of NES (neuralectoderm stem cell) and increased expression of TUBB3, MAP2 and SYN1 (neurons); (Day 15)Generation of 100% electrophysiologycally active neurons, with 20% showing more matured firing patterns, and higher spike amplitude; (Day 15) Increased production of CNTF (ciliary neurotrophic factor); (Day 21) Decreased generation of TBR1+ and FOXG1+ neurons (immature) and increased generation of CTIP2+, SATB2+ and BRN2+ neurons (developed cortical) neurons
Pires and colleagues[28]	ReNcell VM	N2B27 (8 days)	Spun-coated PEDOT:PSS films	5.8×10^{-2} S cm^{-1}	AC, 1 V cm^{-1}, 100 Hz, 12 h on/12 h off.	Decrease in cell aspect ratio. Enhancement of neurite outgrowth. Increase in the number of Tuj1+ cells (neurons) over Gfap+.
Sordini and colleagues[29].	ReNcell-VM, Passage 21	N2B27 (8 days)	Spun-coated PEDOT:PSS films	13 S cm^{-1}	AC (100 Hz), DC (12.5 MHz) and pulsatile DC (100 Hz), 1 V cm^{-1}.	Increased expression (qPCR) of NES and MAP2 with pulsed DC; Increased Tuj1/Gfap ratio (IF) in cultured cells
Tomaskovic-Crook and colleagues[108]	Human iPSCs (ATCC-BXS0116)	STEMdiff™ neural induction media and STEMdiff™ neural progenitor media for "chemical induction" (10 days) mTeSR1 for "no chemical induction" (10 days)	Poly(pyrrole): Dodecylbenzenesulfonate Film	Not calculated	Chemical induction: AC – 0.25 mA cm^{-2}, 8h per day for 3 days No Chemical induction: AC – 0.1 mA cm^{-2}, 8 h per day for 3 days + 0.25 mA cm^{-2} for 8h every 2 days for 6 days	Increased amount of Tuj1, Nestin and Pax6 on cells at day 10 (Chemical induction). Increased expression of neural genes (TUJ1, SYP, GABA, GAD2) and decreased expression of pluripotency genes (OCT4, NANOG)

Table 2 *(Contd.)*

References	Cells used	Differentiation protocol	Substrate composition/type	Substrate electroconductivity	Electrical stimulation protocol	Neural cell profile
Xu and colleagues[25]	hNSC (ReN-VM), Passages 3–5	KnockOut™ DMEM/F12 + StemPro® Neural Supplement + GlutaMAX™-I (7 days)	PANI coated PVV hydrogels	13.27 ± 0.04 mS cm^{-1}	AC – Charged-Balanced biphasic (15, 35 and 75 mV)	Increase in neurite length, proportional to the applied voltages. Increased expression of neural markers (qPCR and Flow cytometry): β3 tubulin, BFABP and PMP22
Yang and colleagues[30]	Human embryonic stem cells	DMEM/F12 (5 days)	Titanium-coated flat and nanopatterned substrates	1250 ± 68 S cm^{-1}	Pulsed electrical stimulation, 1 Hz, 25 V, 3 μA, 30 min, twice a day.	Increase in the number of MAP2+ (qPCR and IF) cells. Increase of the expression of CACNA1C and SCN1α (qPCR). Enhancement of ERK1/2 pathway.
Zhang and colleagues[109]	Heterozygous NRG1-KO or DISC1-LI primary neurons	Conditioned Neurobasal medium	Poly(pyrrole): Dodecylbenzenesulfonate Film	Not calculated	AC, 0.25 mA cm^{-2}, 8h every 24 h for 3 days	NRG1-KO or DISC1-LI neurons were observed to have: 1 – Normalized expression levels (mRNA and protein) of synaptophysin and PSD95; 2 – Increased protein amount of BDNF and MAP2; 3 – No changes in NRG1 and DISC1 protein expression.
Zhu and colleagues[110]	Mouse NSCs (NE-4C)	Not referred (7 days)	Cross-linked poly (acrylonitrile) electrospun fibers	Not calculated, visual demonstration with a circuit	100 μA (asymmetric biphasic)	Increased TUBB3 (qPCR) and MAP2 (qPCR and IF) and decreased expression of GFAP (IF).
This study	iNPCs derived from iPSCs (passage 43)	1 – N2B27 + dual SMAD inhibition (SB-431542 (10 μM) and LDN-193189 (10 nM)) (12 days); 2 – N2B27 (1 day) + FGF2 (3 days) 3 – N2B27 (30 days)	Steps 1 and 2: Tissue culture plate. Step 3: Electrospun coaxial PGS/PCL.PANI fibers	6.3 ± 2.9 × 10^{-2} S cm^{-1}	Pulsative DC, 1 V cm^{-1}, 100 Hz, 12 h on/12 h off.	Increased expression (qPCR) of neural differentiation markers (NEF-H), glutamatergic markers (VGLUT1) and ionic channel components (CACNA1C and SCN1α); Decreased expression (qPCR) of immature/migratory neural markers (TUBB3, DCX) and GABAergic markers (GAD67); Increased amounts of VGLUT1 vs VGAT found by IF on cultured cells.

the expression of MAP2 and ion channel components such as the alpha 1C subunit of the L-type voltage-gated calcium channel (CACNA1C) and the sodium Voltage-Gated Channel Alpha Subunit 1 (SCN1α). Moreover, they suggest that electrical stimulation, through the activation of voltage-sensitive ion channels, enhances the activation of the ERK1/2 pathway and promotes neurogenesis. Other works provide similar results and reach similar conclusions.[31,104–106] However, the long-term effects of electrical stimulation on iPSC neural differentiation and the formation of lineage specific neurons remains to be studied. Moreover, no previous work has addressed the use of coaxial electroconductive fibers as platforms for the long-term neural differentiation of iPSCs under electrical stimulation.

Our results suggest that electrical stimulation of differentiating iNPCs induced unique changes (Table 2). qPCR results indicate that electrical stimulation can promote neural maturation, as evidenced by changes at the mRNA level of TUBB3/NEF and DCX/MAP2/TAU (cytoskeletal remodeling), SYP/CACNA1C/SCN1α (functional maturation) and NEUN (general maturation), and morphological differences between non-stimulated and electrically stimulated neurons. Moreover, lineage-specific changes are promoted by electrical stimulation, including a down-regulation of mRNA of genes specific from GABAergic (GAD67, VGAT) and Dopaminergic (TH) neurons, and an up-regulation of mRNA of genes specific from Glutamatergic neurons (VGLUT1, VGLUT2). Finally, power analysis revealed that the ideal sample size was higher for NEUN ($n = 4$), SYP ($n = 4$), TH ($n = 5$) and VGLUT2 ($n = 11$). Curiously, the p-values (two-tails) for these gene are low [NEUN ($p = 0.061$), SYP ($p = 0.07$), TH ($p = 0.124$), VGLUT2 ($p = 0.185$)]. This suggests that the absence of statistical significance could be underestimated.

Regarding IF, while NEF/NEUN staining confirms the presence of neurons in both the presence and absence of electrical stimulation, VLUT1/VGAT staining reveals striking differences between both conditions. In the absence of electrical stimulation, unaligned and independent VGLUT1+and VGAT+ neurons can be seen, whereas after electrical stimulation there is a predominance of aligned VGAT+ neurons which also co-stain slightly for VGLUT1. When quantified, while VGAT remains constant, VGLUT1 fluorescence is higher in electrical stimulated samples. Following such observations, we hypothesize that the qPCR changes observed for cells exposed to electrical stimulation are occurring in the VGAT+/VGLUT1− neurons, which will differentiate into glutamatergic neurons. The literature also supports this assumption, as previous studies suggest that both VGLUT1 and VGAT transporters can be localized in the same population of cortical neurons and can be active at different stages of neural activity.[111,112] Moreover, co-localization of VGLUT1, VGLUT2 and VGAT was also found in the cerebellar mossy fibers, typically composed by excitatory neurons, whereas VGLUT2 was found in classical GABAergic cerebellar basket cell terminals.[113] Note that in the case of this study the original differentiation protocol of 120 days (17 for neural induction and 103 for neural differentiation) used by Fernandes and colleagues[23] was shortened to 45 days (17 for neural induction and 30 for neural differentiation) to allow to assess, at such culture time point, the potential improvement on efficiency of electrical stimulation of iNPCs cultured on PGS/PCL-PANI fibers. Indeed, the results evidence that electrical stimulation induces changes on neuron phenotype.

For the first time, we show that electrical stimulation switches a neural population from cell population where GABAergic and glutamatergic neurons co-exist to a cell population where GABAergic (VGAT+/VGLUT1−) neurons are absent and there is a predominance of VGAT+/VGLUT1+ neurons. The qPCR results indicate that such neurons are undergoing a shift in maturation to a dominant glutamatergic profile. Moreover, these neurons are potentially functional mature given the striking increase in expression of CACNA1C and SNC1α. Such cell profile would be of interest for applications in numerous cell-based therapy strategies for neurological diseases, including Alzheimer's and other dementia/neurodegeneration associated conditions.

Finally, we believe the full mechanism behind the observed changes needs to be better understood. For example, it is not completely clear whether the switch in neural marker expression from a GABAergic/dopaminergic to a glutamatergic dominant one is a consequence of (a) electrical-induced neural selection from a specific cell pool (*e.g.* apoptosis); (b) enhancement of the differentiation of a specific neural subtype (selective maturation); or (c) acceleration of the differentiation/maturation process (overall maturation). Moreover, the minimum time of stimulation required to induce such changes in the neural population is not known. Finally, the electrophysiologic profile of the obtained neurons need to be assessed to fully confirm neural functionality and lineage. Further studies are required to test these hypotheses.

5. Conclusion

In the present work, electroconductive coaxial fibers composed of PCL-PANI as the shell and PGS as the core were produced. The coaxial fibers obtained are electroconductive, hydrophilic, highly porous, able to swell up to two times their weight and have a Young's modulus compatible with NSC culture. The coaxial fibers obtained are stable in PBS, being able to maintain significant electroconductivity for up to 28 days. In the presence of lipase, PGS/PCL-PANI core layer PGS degrades completely after 7 days, but the shell layer (electroconductive) degrades slower. iPSCs, after neural induction, were successfully differentiated into neurons on PGS/PCL-PANI coaxial fibers. These fibers allowed the cells to express characteristic neural markers and also mature neural markers (GAD67 and TH). Electrical stimulation of differentiating neurons induces the formation of long and parallel axonal fibers, a switch from the characteristic GABAergic dominant profile to a more glutamatergic profile and promotes neural maturation. In particular, we observe by qPCR the expression of higher levels of

synaptophysin (pre-synaptic vesicles), NEF-H (larger caliber axons), CACNA1C (calcium channels), SCN1α (sodium channels) and VGLUT1 (glutamatergic neurons), accompanied by a decrease in DCX (migratory early neurons), TUBB3 (early-neural marker) and GAD67 (GABAergic neurons). By IF, we observe a shift from the co-existence of VGAT+ and VGLUT1+ neurons to ones with VGAT+/VGLUT1+ co-staining. These coaxial fibers can therefore be used in the design of platforms for the electrical stimulation to differentiate neural cells for the treatment of neurological diseases.

Author contributions

Conceptualization: FFFG, FCF and RJL. Project administration: FFFG. Methodology, Investigation and Validation: FFFG assisted by DESN and CAVR (iPSC culture and neural differentiation), FAF (PGS synthesis), PP and RC (Mechanical properties assessment) ACM (FTIR analysis), JM (electroconductivity measurements) and FCF (stability and biodegradation assays). Formal analysis: FFFG. Visualization: FFFG, DESN, CAVR. Funding Acquisition and Resources: RC, ACM, JMSC, JM, FCF and RJL. Manuscript Writing: FFFG. Manuscript Revision and Editing: all the authors.

Conflicts of interest

The authors declare that they have no known competing financial interests or personal relationships that could have appeared to influence the work reported in this paper.

Acknowledgements

The authors dedicate this paper to the memory of P. Paradiso. The authors acknowledge the help of MD Isabel Nogueira for SEM image acquisition, BScs Caitlyn Chapman and Pauline Hoffman for their help in the initial electrospinning optimization, both Dr Ranodhi Udangawa Keating and Mr Charles Willard for the electrospinning setup images used here, the PhD student Mário Vale for FTIR data acquisition and Dr Evguenia Bekman for the valuable discussion over of the main cellular findings and important for the conclusion of this work.

A special thanks to Dr Paiyz E Mikael and Dr João C Silva for electrospinning troubleshooting, and to Prof Tiago Fernandes, Dr Cláudia Miranda, Dr Ana Rita Gomes, Dr Teresa Silva and Dr Marta Carvalho for troubleshooting over the neural differentiation protocol.

Funding received from FCT – Portuguese Funding for Science and Technology, specifically through the dedicated funding of Fábio F.F. Garrudo scholarship PD/BD/114045/2015, Diogo E. S. Nogueira scholarship PD/BD/128376/2017, project NEURON (PTDC/CTM-CTM/30237/2017) and Project Stimuli2BioScaffold (PTDC/EME-SIS/032554/2017, POCI-01-0145-FEDER-32554) is acknowledged. Additional funding from FCT through iBB – Institute for Bioengineering and Biosciences (UID/BIO/04565/2021), Instituto de Telecomunicações (UIDB/50008/2020), CERENA (UIDB/04028/2020) and IDMEC – Instituto de Engenharia Mecânica (LAETA, project UIDB/50022/2020). We also acknowledge the funding received from POR de Lisboa 2020 through the project PRECISE – Accelerating progress toward the new era of precision medicine (Project No. 16394). This work is also funded by the US National Institutes of Health, grant # DK111958 and New York State grant # SCRIB DOH01-PART2-2017.

References

1 S. Mehmood, M. Bilal, R. Manzoor and H. M. N. Iqbal, *Mater. Today Chem.*, 2019, **13**, 88–97.
2 H.-H. Suzana, *Front. Hum. Neurosci.*, 2009, **3**, 31.
3 E. Altun, M. Aydogdu, S. Togay, A. Sengil, N. Ekren, M. Haskoylu, E. Oner, N. Altuncu, G. Ozturk, M. Crabbe-Mann, J. Ahmed, O. Gunduz and M. Edirisinghe, *Eur. Polym. J.*, 2019, **114**, 98–108.
4 F. Chaudhry, R. Reimer, E. Bellocchio, N. Danbolt, K. Osen, R. Edwards and J. Storm-Mathisen, *J. Neurosci.*, 1998, **18**, 9733–9750.
5 S. Fung, M. Webster, C. Weickert and C. Weicker, *Brain Res.*, 2011, **1388**, 22–31.
6 M. Morales and D. H. Root, *Neuroscience*, 2014, **282**, 60–68.
7 P. Roach, T. Parker, N. Gadegaard and M. Alexander, *Biomater. Sci.*, 2012, **1**, 83–93.
8 J. Wu, L. Xie, W. Lin and Q. Chen, *Drug Discov. Today*, 2017, **22**, 1375–1384.
9 J. Harberts, U. Haferkamp, S. Haugg, C. Fendler, D. Lam, R. Zierold, O. Pless and R. Blick, *Biomater. Sci.*, 2020, **8**, 2434–2446.
10 B. Mammadov, M. Sever, M. Guler and A. Tekinay, *Biomater. Sci.*, 2013, **1**, 1119–1137.
11 S. Knowlton, Y. Cho, X.-J. Li, A. Khademhosseini and S. Tasoglu, *Biomater. Sci.*, 2016, **4**, 768–784.
12 J. Du, H. Chen, L. Qing, X. Yang and X. Jia, *Biomater. Sci.*, 2018, **6**, 1299–1311.
13 K. Shimba, C.-H. Chang, T. Asahina, F. Moriya, K. Kotani, Y. Jimbo, A. Gladkov, O. Antipova, Y. Pigareva, V. Kolpakov, I. Mukhina, V. Kazantsev and A. Pimashkin, *Front. Neurosci.*, 2019, **13**, 890.
14 K. Takahashi, K. Tanabe, M. Ohnuki, M. Narita, T. Ichisaka, K. Tomoda and S. Yamanaka, *Cell*, 2007, **131**, 861–872.
15 J. Yu, M. Vodyanik, K. Smuga-Otto, J. Antosiewicz-Bourget, J. Frane, S. Tian, J. Nie, G. Jonsdottir, V. Ruotti, R. Stewart, I. Slukvin and J. Thomson, *Science*, 2007, **318**, 1917–1920.
16 Y. Shi, P. Kirwan and F. Livesey, *Nat. Protoc.*, 2012, **7**, 1836.
17 S. P. Paşca, T. Portmann, I. Voineagu, M. Yazawa, A. Shcheglovitov, A. M. Paşca, B. Cord, T. D. Palmer, S. Chikahisa, S. Nishino, J. A. Bernstein, J. Hallmayer, D. H. Geschwind and R. E. Dolmetsch, *Nat. Med.*, 2011, **17**, 1657–1662.

18 N. Farra, W.-B. Zhang, P. Pasceri, J. Eubanks, M. Salter and J. Ellis, *Mol. Psychiatry*, 2012, **17**, 1261.
19 K. M. Haston and S. Finkbeiner, *Annu. Rev. Pharmacol. Toxicol.*, 2016, **56**, 489–510.
20 T. Julia, *Neurosci. Lett.*, 2019, **699**, 31–40.
21 P. Ni, H. Noh, Z. Shao, Q. Zhu, Y. Guan, J. Park, F. Arif, J. Park, C. Abani, C. Beaudreault, J. Park, E. Berry, A. Moghadam, P. Stanton, J. Hutchinson, B. Andrews, C. Faux, J. Parnevelas, L. Eisenberg, K. Park, V. Bolshakov and S. Chung, *Mol. Ther. – Methods Clin. Dev.*, 2019, **13**, 414–430.
22 F. Bianchi, M. Malboubi, Y. Li, J. George, A. Jerusalem, F. Szele, M. Thompson and H. Ye, *Stem Cell Res.*, 2018, **32**, 126–134.
23 T. G. Fernandes, S. T. Duarte, M. Ghazvini, C. Gaspar, D. C. Santos, A. R. Porteira, G. M. Rodrigues, S. Haupt, D. M. Rombo, J. Armstrong, A. M. Sebastião, J. Gribnau, À. Garcia-Cazorla, O. Brüstle, D. Henrique, J. M. Cabral and M. Diogo, *Biotechnol. J.*, 2015, **10**, 1578–1588.
24 L. Ghasemi-Mobarakeh, M. P. Prabhakaran, M. Morshed, M. H. Nasr-Esfahani and S. Ramakrishna, *Tissue Eng. Part A*, 2009, **15**, 3605–3619.
25 B. Xu, T. Bai, A. Sinclair, W. Wang, Q. Wu, F. Gao, H. Jia, S. Jiang and W. Liu, *Mater. Today Chem.*, 2016, **1**, 15–22.
26 A. N. Koppes, N. W. Zaccor, C. J. Rivet, L. A. Williams, J. M. Piselli, R. J. Gilbert and D. M. Thompson, *J. Neural Eng.*, 2014, **11**, 046002.
27 S. Song, D. Amores, C. Chen, K. McConnell, B. Oh, A. Poon and P. George, *Sci. Rep.*, 2019, **9**, 19565.
28 F. Pires, Q. Ferreira, C. Rodrigues, J. Morgado and F. Ferreira, *Biochim. Biophys. Acta, Gen. Subj.*, 2015, **1850**, 1158–1168.
29 L. Sordini, F. F. F. Garrudo, C. Rodrigues, R. J. Linhardt, J. M. S. Cabral, F. C. Ferreira and J. Morgado, *Front. Bioeng. Biotechnol.*, 2021, **9**, 73.
30 K. Yang, S. Yu, J. Lee, H.-R. Lee, G.-E. Chang, J. Seo, T. Lee, E. Cheong, S. Im and S.-W. Cho, *Nanoscale*, 2017, **9**, 18737–18752.
31 F. Garrudo, P. E. Mikael, C. Rodrigues, R. W. Udangawa, P. Paradiso, C. A. Chapman, P. Hoffman, R. Colaço, J. Cabral, J. Morgado, R. J. Linhardt and F. Ferreira, *Mater. Sci. Eng. C*, 2021, **120**, 111680.
32 K. Woeppel, Q. Yang and X. Cui, *Curr. Opin. Biomed. Eng.*, 2017, **4**, 21–31.
33 S. Khan and A. Narula, *Eur. Polym. J.*, 2016, **81**, 161–172.
34 N. Alba, Z. Du, K. Catt, T. Kozai and X. Cui, *Biosensors*, 2015, **5**, 618–646.
35 D. Heo, S.-J. Lee, R. Timsina, X. Qiu, N. J. Castro and L. G. Zhang, *Mater. Sci. Eng., C*, 2019, **99**, 582–590.
36 F. F. F. Garrudo, R. N. Udangawa, P. R. Hoffman, L. Sordini, C. A. Chapman, P. E. Mikael, F. A. Ferreira, J. C. Silva, C. A. V. Rodrigues, J. M. S. Cabral, J. M. F. Morgado, F. C. Ferreira and R. J. Linhardt, *Mater. Today Chem.*, 2019, **14**, 100185.
37 A. Carlson, N. Bennett, N. Francis, A. Halikere, S. Clarke, J. Moore, R. Hart, K. Paradiso, M. Wernig, J. Kohn, Z. Pang and P. Moghe, *Nat. Commun.*, 2016, **7**, 10862.
38 C. Madl, B. LeSavage, C. Dinh, R. Dewi, R. Stowers, M. Khariton, K. Lampe, D. Nguyen, O. Chaudhuri, A. Enejder and S. Heilshorn, *Nat. Mater.*, 2017, **16**, 1233.
39 C. M. Madl, B. L. LeSavage, R. E. Dewi, K. J. Lampe and S. C. Heilshorn, *Adv. Sci.*, 2019, **6**, 1801716.
40 X. Loh, A. Karim and C. Owh, *J. Mater. Chem. B*, 2015, **3**, 7641–7652.
41 Y. Ikada and H. Tsuji, *Macromol. Rapid Commun.*, 2000, **21**, 117–132.
42 D. Nisbet, A. Rodda, M. Horne, J. Forsythe and D. Finkelstein, *Biomaterials*, 2009, **30**, 4573–4580.
43 L. Jin, B. Hu, Z. Li, J. Li, Y. Gao, Z. Wang and J. Hao, *ACS Appl. Mater. Interfaces*, 2018, **10**, 18543–18550.
44 Y. Jiao, C. Li, L. Liu, F. Wang, X. Liu, J. Mao and L. Wang, *Biomater. Sci.*, 2020, **8**, 3574–3600.
45 F. Garrudo, P. Mikael, K. Xia, J. Silva, Y. Ouyang, C. Chapman, P. Hoffman, Y. Yu, X. Han, C. Rodrigues, J. Cabral, J. Morgado, F. Ferreira and R. Linhardt, *Biochimie*, 2021, **182**, 61–72.
46 M. Maldonado, L. Wong, C. Echeverria, G. Ico, K. Low, T. Fujimoto, J. Johnson and J. Nam, *Biomaterials*, 2015, **50**, 10–19.
47 D. Sridharan, A. Palaniappan, B. Blackstone, J. Dougherty, N. Kumar, P. Seshagiri, N. Sayed, H. Powell and M. Khan, *Mater. Sci. Eng., C*, 2021, **118**, 111354.
48 N. Mohtaram, J. Ko, C. King, L. Sun, N. Muller, M. Jun and S. Willerth, *J. Biomed. Mater. Res., Part A*, 2015, **103**, 2591–2601.
49 K. Lang, S. Bhattacharya, Z. Ning, R. Sánchez-Leija, M. Bramson, R. Centore, D. Corr, R. Linhardt and R. Gross, *Biomacromolecules*, 2020, **21**, 3197–3206.
50 L. Hou, W. Udangawa, A. Pochiraju, W. Dong, Y. Zheng, R. Linhardt and T. Simmons, *ACS Biomater. Sci. Eng.*, 2016, **2**, 1905–1913.
51 W. Udangawa, C. Willard, C. Mancinelli, C. Chapman, R. Linhardt and T. Simmons, *Cellulose*, 2019, **26**, 1855–1868.
52 L. Binan, C. Tendey, G. Crescenzo, R. Ayoubi, A. Ajji and M. Jolicoeur, *Biomaterials*, 2014, **35**, 664–674.
53 J. W. Drexler and H. M. Powell, *Acta Biomater.*, 2011, **7**, 1133–1139.
54 P. Rathore and J. D. Schiffman, *ACS Appl. Mater. Interfaces*, 2021, **13**, 48–66.
55 J. Xie, M. MacEwan, S. Willerth, X. Li, D. Moran, S. Sakiyama-Elbert and Y. Xia, *Adv. Funct. Mater.*, 2009, **19**, 2312–2318.
56 J. Zhang, K. Qiu, B. Sun, J. Fang, K. Zhang, H. EI-Hamshary, S. S. Al-Deyab and X. Mo, *J. Mater. Chem. B*, 2014, **2**, 7945–7954.
57 R. Borah, G. Ingavle, S. Sandeman, A. Kumar and S. Mikhalovsky, *Biomater. Sci.*, 2018, **6**, 2342–2359.
58 J. Silva, R. Udangawa, J. Chen, C. Mancinelli, F. Garrudo, P. Mikael, J. Cabral, F. Ferreira and R. Linhardt, *Mater. Sci. Eng., C*, 2019, **107**, 110291.
59 L. Hou, X. Zhang, P. Mikael, L. Lin, W. Dong, Y. Zheng, T. Simmons, F. Zhang and R. Linhardt, *ACS Omega*, 2017, **2**, 6321–6328.

60 F. F. F. Garrudo, C. A. Chapman, P. R. Hoffman, R. W. Udangawa, J. C. Silva, P. E. Mikael, C. A. V. Rodrigues, J. M. S. Cabral, J. M. F. Morgado, F. C. Ferreira and R. J. Linhardt, *Eur. Polym. J.*, 2019, **117**, 28–37.
61 S. Chambers, C. Fasano, E. Papapetrou, M. Tomishima, M. Sadelain and L. Studer, *Nat. Biotechnol.*, 2009, **27**, 275–280.
62 C. Rodrigues, M. Diogo, C. Silva and J. Cabral, *Biotechnol. Appl. Biochem.*, 2011, **58**, 231–242.
63 D. Nogueira, C. Rodrigues, M. Carvalho, C. Miranda, Y. Hashimura, S. Jung, B. Lee and J. Cabral, *J. Biol. Eng.*, 2019, **13**, 74.
64 T. Silva, E. Bekman, T. Fernandes, S. Vaz, C. Rodrigues, M. Diogo, J. Cabral and M. Carmo-Fonseca, *Front. Bioeng. Biotechnol.*, 2020, **8**, 70.
65 T. H. Qazi, R. Rai, D. Dippold, J. E. Roether, D. W. Schubert, E. Rosellini, N. Barbani and A. R. Boccaccini, *Acta Biomater.*, 2014, **10**, 2434–2445.
66 S. Ghafaralahi, M. Ebrahimian-Hosseinabadi and A. Kharazi, *J. Bioact. Compat. Polym.*, 2018, **33**, 529–542.
67 H. Alharbi, M. Luqman, K. Khalil, Y. Elnakady, O. Abd-Elkader, A. Rady, N. Alharthi and M. Karim, *Eur. Polym. J.*, 2018, **98**, 483–491.
68 M. Iglesias-Echevarria, L. Durante, R. Johnson, M. Rafuse, Y. Ding, W. Bonani, D. Maniglio and W. Tan, *Biomater. Sci.*, 2019, **7**, 3640–3651.
69 M. Solazzo, K. Krukiewicz, A. Zhussupbekova, K. Fleischer, M. Biggs and M. Monaghan, *J. Mater. Chem. B*, 2019, **7**, 4811–4820.
70 H. Yang, B. Lee, J. Tsui, J. Macadangdang, S. Jang, S. Im and D. Kim, *Adv. Healthcare Mater.*, 2016, **5**, 137–145.
71 J. Shin, E. Choi, J. Cho, A.-N. Cho, Y. Jin, K. Yang, C. Song and S.-W. Cho, *Biomacromolecules*, 2017, **18**, 3060–3072.
72 E. Aurand, J. Wagner, C. Lanning and K. Bjugstad, *J. Funct. Biomater.*, 2012, **3**, 839–863.
73 K. Menzies and L. Jones, *Optometry Vision Sci.*, 2010, **87**, 387–399.
74 L. Tian, M. P. Prabhakaran, J. Hu, M. Chen, F. Besenbacher and S. Ramakrishna, *Colloids Surf., B*, 2016, **145**, 420–429.
75 N. Blinova, J. Stejskal, M. Trchová and J. Prokeš, *Polym. Int.*, 2008, **57**, 66–69.
76 A. R. Hopkins and P. G. Rasmussen, *Macromolecules*, 1996, **29**, 7838–7846.
77 C. Englund, A. Fink, C. Lau, D. Pham, R. Daza, A. Bulfone, T. Kowalczyk and R. Hevner, *J. Neurosci.*, 2005, **25**, 247–251.
78 J. G. Gleeson, P. T. Lin, L. A. Flanagan and C. A. Walsh, *Neuron*, 1999, **23**, 257–271.
79 L. Dehmelt and S. Halpain, *Genome Biol.*, 2004, **6**, 204.
80 P. N. Hoffman, D. W. Cleveland, J. W. Griffin, P. W. Landes, N. J. Cowan and D. L. Price, *Proc. Natl. Acad. Sci. U. S. A.*, 1987, **84**, 3472–3476.
81 Q. Zhang, S. Beirne, K. Shu, D. Esrafilzadeh, X.-F. Huang and G. Wallace, *Sci. Rep.*, 2018, **8**, 9855.
82 W. Khalil, T. Tiraihi, M. Soleimani, N. Baheiraei and K. Zibara, *Neurotox Res.*, 2020, **38**, 707–722.
83 Y. Setty, C.-C. Chen, M. Secrier, N. Skoblov, D. Kalamatianos and S. Emmott, *BMC Syst. Biol.*, 2011, **5**, 154.
84 G. Christopherson, H. Song and H.-Q. Mao, *Biomaterials*, 2009, **30**, 556–564.
85 H. Wang, M. Mullins, J. Cregg, C. McCarthy and R. Gilbert, *Acta Biomater.*, 2010, **6**, 2970–2978.
86 C. D. L. Johnson, J. M. Zuidema, K. R. Kearns, A. B. Maguire, G. P. Desmond, D. M. Thompson and R. J. Gilbert, *ACS Appl. Biol. Mater.*, 2019, **2**, 104–117.
87 S. Ankam, M. Suryana, L. Chan, A. Moe, B. Teo, J. Law, M. Sheetz, H. Low and E. Yim, *Acta Biomater.*, 2013, **9**, 4535–4545.
88 S. Ankam, C. Lim and E. Yim, *Biomaterials*, 2015, **47**, 20–28.
89 A. Engler, S. Sen, H. Sweeney and D. Discher, *Cell*, 2006, **126**, 677–689.
90 M. Nogueira, O. Lafitte, J.-M. Steyaert, H. Bakardjian, B. Dubois, H. Hampel and L. Schwartz, *Alzheimers Dement*, 2016, **12**, 11–20.
91 A. Saudi, S. Amini, N. Amirpour, M. Kazemi, A. Kharazi, H. Salehi and M. Rafienia, *Mater. Sci. Eng., C*, 2019, **104**, 110005.
92 A. Saudi, M. Rafienia, A. Kharazi, H. Salehi, A. Zarrabi and M. Karevan, *Polym. Adv. Technol.*, 2019, **30**, 1427–1440.
93 M. Prabha, V. Ravi and N. Swamy, *Indian J. Clin. Biochem.*, 2013, **28**, 283–291.
94 W. Dong, H. Gong, G. Zhang, S. Vuletic, J. Albers, J. Zhang, H. Liang, Y. Sui and J. Zheng, *Acta Biochem. Biophys. Sin*, 2016, **49**, 62–73.
95 H. Chahiniana and L. Sarda, *Protein. Pept. Lett.*, 2009, **16**, 1149–1161.
96 P.-P. He, T. Jiang, X.-P. OuYang, Y.-Q. Liang, J.-Q. Zou, Y. Wang, Q.-Q. Shen, L. Liao and X.-L. Zheng, *Clin. Chim. Acta*, 2018, **480**, 126–137.
97 C. Cruciani-Guglielmacci and C. Magnan, *Biochimie*, 2017, **143**, 51–55.
98 S.-G. Hong, H. Kim and J. Kim, *Langmuir*, 2014, **30**, 911–915.
99 S. Soni, B. Dwivedee and U. Banerjee, *Int. J. Biol. Macromol.*, 2020, **161**, 573–586.
100 Y.-C. Kuo and Y.-H. Chang, *Colloids Surf., B*, 2013, **102**, 405–411.
101 L. Fan, C. Liu, X. Chen, Y. Zou, Z. Zhou, C. Lin, G. Tan, L. Zhou, C. Ning and Q. Wang, *ACS Appl. Mater. Interfaces*, 2018, **10**, 17742–17755.
102 H. Rhee, A. H. Shaib, K. Rehbach, C. Lee, P. Seif, C. Thomas, E. Gideons, A. Guenther, T. Krutenko, M. Hebisch, M. Peitz, N. Brose, O. Brüstle and J. Rhee, *Cell. Rep.*, 2019, **27**, 2212–2228.e7.
103 S. Wang, S. Guan, J. Xu, W. Li, D. Ge, C. Sun, T. Liu and X. Ma, *Biomater. Sci.*, 2017, **5**, 2024–2034.
104 C. Chen, X. Bai, Y. Ding and I.-S. Lee, *Biomater. Res.*, 2019, **23**, 25.

105 T. Brushart, P. Hoffman, R. Royall, B. Murinson, C. Witzel and T. Gordon, *J. Neurosci.*, 2002, **22**, 6631–6638.
106 X. Quan, L. Huang, Y. Yang, T. Ma, Z. Liu, J. Ge, J. Huang and Z. Luo, *Neurochem. Res.*, 2017, **42**, 513–525.
107 B. Oh, Y. Wu, V. Swaminathan, V. Lam, J. Ding and P. M. George, *Adv Sci.*, 2021, **8**, 2002112.
108 E. Tomaskovic-Crook, Q. Gu, S. Rahim, G. Wallace and J. Crook, *Cells*, 2020, **9**, 658.
109 Q. Zhang, D. Esrafilzadeh, J. Crook, R. Kapsa, E. Stewart, E. Tomaskovic-Crook, G. Wallace and X.-F. Huang, *Sci. Rep.*, 2017, **7**, 42525.
110 W. Zhu, T. Ye, S.-J. Lee, H. Cui, S. Miao, X. Zhou, D. Shuai and L. Zhang, *Nanomedicine*, 2017, **14**, 2485–2494.
111 G. Fattorini, C. Verderio, M. Melone, S. Giovedì, F. Benfenati, M. Matteoli and F. Conti, *J. Neurochem.*, 2009, **110**, 1538–1546.
112 G. Fattorini, F. Antonucci, E. Menna, M. Matteoli and F. Conti, *J. Cell Sci.*, 2015, **128**, 1669–1673.
113 J.-F. Zander, A. Münster-Wandowski, I. Brunk, I. Pahner, G. Gómez-Lira, U. Heinemann, R. Gutiérrez, G. Laube and G. Ahnert-Hilger, *J. Neurosci.*, 2010, **30**, 7634–7645.

